Chapter 1

Introduction

The theory of elementary particles, the Standard Model of Particle Physics, is an incredibly successful theory which has stood up to every experimental test since it was first formulated in the 1970s [1, 2]. The recent discovery of the Higgs boson at CERN [3, 4] was the final missing piece and establishes the Standard Model as *the* theory of physical phenomena at the electroweak scale (up to a few hundred GeV) [5, 6].

There are however plenty of shortcomings of the theory and further theoretical and experimental work is necessary to advance our understanding of fundamental physics [7]. For example, it ignores gravity and requires a quantised theory of gravity to reconcile it with General Relativity. The observation of 'Dark Matter' and 'Dark Energy' in Astrophysics and Cosmology cannot be explained using the known particles in the Standard Model and needs an extension of the theory. It also offers no convincing explanation of the observed domination of matter over antimatter evident in the Universe, given they were created equally in the Big Bang. Additionally, there are many unresolved theoretical problems within the Standard Model, evidence of a more fundamental underlying theory which may replace it. It is for this reason that experiments are hoping to find phenomena which may only be understood 'Beyond the Standard Model'.

Neutrinos offer the most promising possibilities of new physics and are currently the subject of a great amount of research [6]. The observation of neutrino oscillations [8, 9], along with the associated implication of neutrino mass, represents physics which was not included in, or predicted by, the Standard Model. In recent years the field of neutrino physics has advanced rapidly and there is currently good understanding of most experimental results. Open questions remain, such as the origin and nature of neutrino mass, the characteristics of neutrino interactions and the exact features of neutrino mixing, and will define the future of the field for many years to come. This will be discussed in more detail in Chapter 2. There is also the possibility neutrinos may explain the aforementioned matter-antimatter

asymmetry through CP-violation in the lepton sector and may even provide a potential dark matter candidate in the possible sterile neutrino.

Future understanding and discoveries in neutrino physics requires precise measurements from highly sensitive experiments. The future Deep Underground Neutrino Experiment (DUNE) is such an experiment and will be able to contribute towards many of the unanswered questions in the field. The DUNE experiment, along with its sensitivities to unexplained phenomena, is the subject of Chapter 3. It will use large quantities of liquid argon in order to make the necessary precision measurements and will be the largest experiment using this technology ever built by an order of magnitude. In order to ensure the experiment is successful and reaches its physics potential, prototyping the technology and detector design is essential. The experiences of operating such a prototype, the 35 ton experiment, is discussed in Chapter 4, and additionally in Chapter 6.

A major challenge in the design choice of DUNE is the successful and detailed reconstruction of particle interactions necessary to make the required measurements. This is discussed in depth in Chapter 5, with emphasis placed on the difficult task of reconstructing showering particles. The performance of the reconstruction in the selection of the main signal events for DUNE, and an analysis, at this early stage, of the current status of the DUNE software at meeting its required physics goals is presented in Chapter 8.

Happy to remove this paragraph if you want – since I've mixed up previous work with my contributions (particularly in reconstruction) I thought it may be good to explicitly point out. The author contributed directly to the success of the 35 ton experiment (Chapter 4) and developed the reconstruction described in Sections 5.3 and 5.4 within Chapter 5. The content presented in Chapters 6, 7 and 8 is all original work.

Chapter 2

Neutrino Physics

This chapter contains an introduction to the field of neutrino physics to provide context for the main work presented in this thesis. The history of neutrino physics is an interesting story in its own right and provides the foundation for the present and future of the field. This will be briefly retold in Section 2.1 and will motivate a discussion of neutrino oscillations in Section 2.2. An overview of the current status of the field and its future is contained in Section 2.3.

2.1 Historical Context

2.1.1 Prediction of the Neutrino

The neutrino was first postulated in 1930 by Wolfgang Pauli [10] in order to account for an inconsistency in the theory of β-decay. In the apparent two-body decay

$$A \to B + e^{-}, \tag{2.1}$$

kinematically the electron must be emitted with an energy given by

$$E = \left(\frac{m_A^2 - m_B^2 + m_e^2}{2m_A} \right) c^2, \tag{2.2}$$

where m_α is the mass of particle α. This energy is fixed given the masses of the particles; it was observed however that the electron energy followed a distribution (Figure 2.1), with Equation 2.2 giving the maximum permitted energy. The neutrino was postulated as a third final state particle in order to account for this result and retain energy conservation laws. Pauli initially called the particle a *neutron* (preempting the name Chadwick was to give his

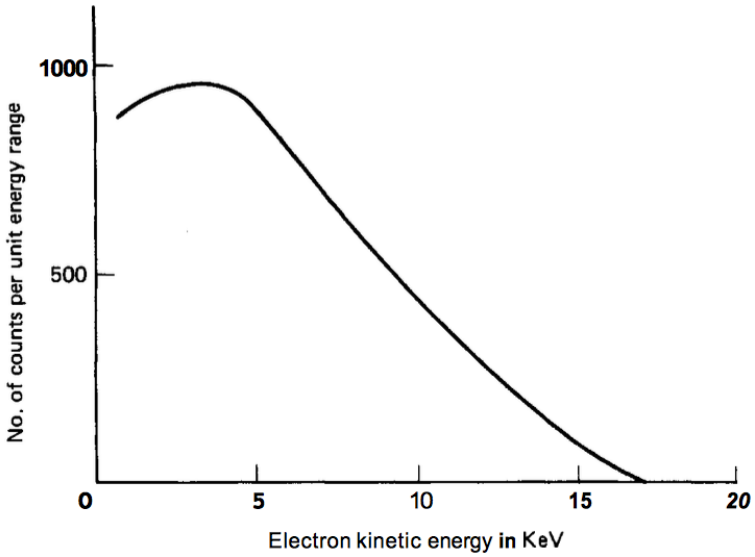

Fig. 2.1 Energy spectrum of the electron produced in beta decay [14].

discovered particle in 1932) but his idea was met with much scepticism. It was Fermi who named the new particle *neutrino* ('little neutral one') when incorporating Pauli's hypothesis into his theory of beta decay [11–13]. With the huge success and acceptance of this theory, the field of neutrino physics was born.

Further indications of the existence of the neutrino were provided by the studies of pion and muon decay by Cecil Powell's group at Bristol in 1947 [15, 16]. Topological investigations of the newly discovered π meson and its apparent decay into a lighter meson (now known to actually be the muon lepton) appear to hint at the presence of an additional, unknown, daughter particle [15]. Furthermore, subsequent studies of the decay of the muons implied a three-body decay involving two unknown final state particles, analogous to the implication of the neutrino in β-decay by considering the electron energy distribution [17]. It seemed a model involving neutrinos could explain these observations and provided more suggestions for the existence of such a particle.

2.1.2 Discovery of the Neutrino

The elegance of Fermi's theory convinced many physicists of the existence of the neutrino but until discovered experimentally it remained a hypothetical 'bookkeeping' device. Given the elusive nature of neutrinos this was not for many years, leading to Pauli famously declaring "I have done a terrible thing. I have postulated a particle that cannot be detected". However, a series of experiments conducted between 1953 and 1956 by Clyde Cowan and Frederick Reines confirmed the hypothesis and were later rewarded with the Nobel Prize in Physics

in 1995. Using the new technology of liquid scintillator detectors [18], they designed an experiment [19] to study the (anti)neutrinos produced in inverse beta decay

$$\bar{\nu}_e + p \rightarrow e^+ + n \tag{2.3}$$

in the Hanford nuclear reactor in Washington, U.S.A. Their signal comprised of an initial release of scintillation light when the positron annihilates with an electron, followed a characteristic time later by a gamma ray corresponding to the neutron capture. The initial results from 1953 [20] hinted at an excess over predicted background but the background proved to be much larger than anticipated, mainly due to an underestimation of the effects of cosmic rays. A second experiment was conducted in 1956, this time 12 m underground and 11 m from the Savannah River reactor in South Carolina. A neutrino detection rate of 2.9$\pm$0.2 per hour, greater than 20 times the accidental background rate was reported, confirming the previous indications [21]. The experimental discovery of the neutrino was confirmed. [Bit more description? – Describe detector, method for detecting positron.]

Ray Davis was also using nuclear reactors to study the interaction rates of neutrinos. Using a detector comprised of 3000 gallons of carbon tetrachloride (CCl_4) also close to the Savannah River reactor, Davis and Harmer searched for the interactions

$$\bar{\nu} + \mathrm{Cl}^{37} \rightarrow \mathrm{Ar}^{37} + e^- \qquad (\bar{\nu} + n \rightarrow p^+ + e^-). \tag{2.4}$$

Since it was known from Reines and Cowan that inverse beta decay

$$\nu + \mathrm{Cl}^{37} \rightarrow \mathrm{Ar}^{37} + e^- \qquad (\nu + n \rightarrow p^+ + e^-) \tag{2.5}$$

occurs, this facilitated a comparison between the neutrino and the antineutrino. They found the interaction shown in Equation 2.4 occurred at a rate less than 20 times that represented in Equation 2.5, implying for the first time a difference between neutrinos and antineutrinos [22]. This gave rise to the notion of 'lepton number' and its conservation in physical interactions.

It was few years before the next chapter in the history of neutrinos, the discovery of the muon neutrino in 1962 at Brookhaven [23]. It was noted the apparently permitted decay

$$\mu^- \not\rightarrow e^- + \gamma \tag{2.6}$$

is never observed, inciting the possibility of two distinct neutrinos. In order to test this, Lederman, Schwarz and Steinberger used a muon neutrino beam to look for two separate

interactions:

$$\bar{\nu}_\mu + p^+ \rightarrow \mu^+ + n, \tag{2.7}$$

$$\bar{\nu}_\mu + p^+ \rightarrow e^+ + n. \tag{2.8}$$

With only one type of neutrino, each interaction would be expected to occur at around the same rate. The beam was produced by accelerating protons up to 15 GeV and using a Beryllium target to create secondary mesons, decaying to produce neutrinos with energies up to 1 GeV. 34 muon tracks were detected (with an estimated background from cosmic muons of 5) and no events consistent with electrons were observed. This remarkable result can only be rivalled by the technological advancements required; it was the first experiment to construct and use an artificial neutrino beam (common to all contemporary long-baseline experiments) and used 13.5 m thick steel from a dismantled battleship in order to ensure only neutrinos arrived at the spark chamber detector. This discovery was rewarded with the Nobel Prize in 1988.

A third generation of lepton, the τ, was discovered in 1975 by Martin Perl and his team at SLAC [24], completing the set of three charged leptons. They reported 64 events of the form

$$e^+ + e^- \rightarrow e^\pm + \mu^\mp + \geq 2 \text{ undetected particles}, \tag{2.9}$$

using the energy and angle distributions to predict at least two additional particles. They claimed 'no conventional explanation' could account for these events and proposed the existence of a heavier charged lepton as an intermediate stage:

$$e^+ + e^- \rightarrow \tau^+ + \tau^- \rightarrow e^\pm + \mu^\mp + 4\nu. \tag{2.10}$$

The τ lepton was subsequently characterised by further experiments by the Mark I detector at SLAC [25] and by the PLUTO collaboration at DESY [26]. This result heavily implied the existence of an associated neutrino to complete the symmetry observed in the first two lepton couplets.

Further evidence for a third neutrino was provided by four experiments using the Large Electron-Positron Collider (LEP) at CERN in 1989 which were studying the production of the newly discovered Z^0 boson [27–30]. The width Γ_Z of the Z^0 resonance is dependent on the partial widths relating to final state charged leptons, hadrons and neutrinos;

$$\Gamma_Z = N_\nu \Gamma_\nu + 3\Gamma_{ee} + \Gamma_{\text{hadron}}, \tag{2.11}$$

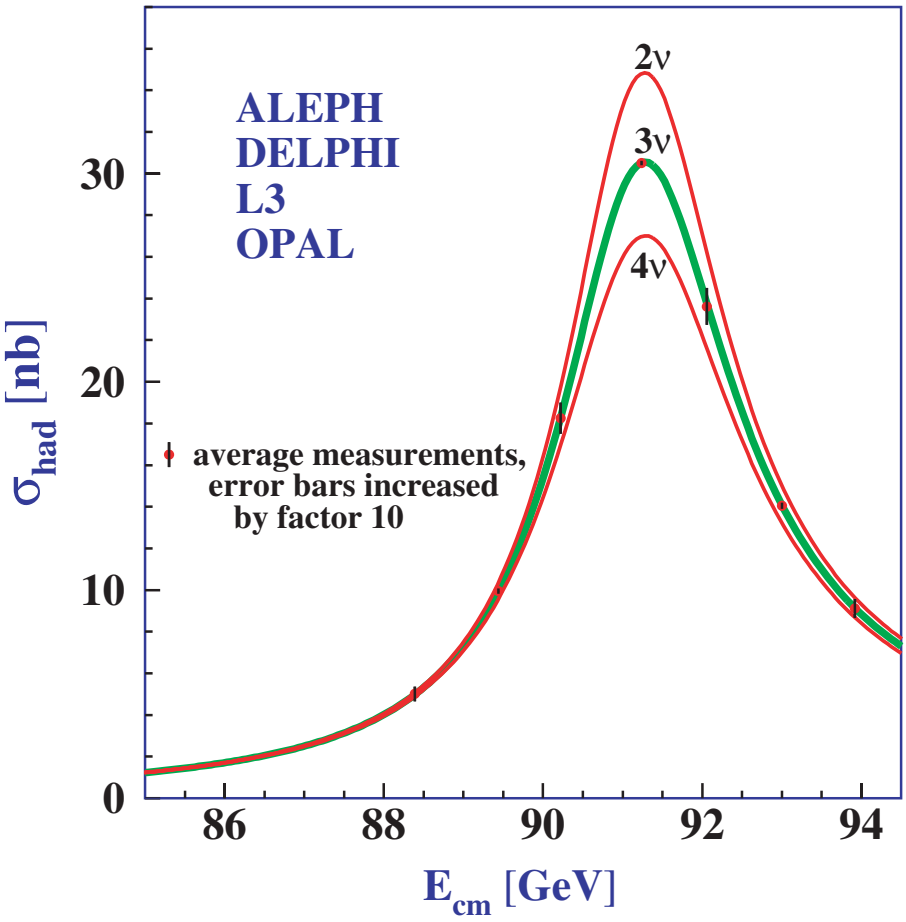

Fig. 2.2 Measurements of the hadron production cross-section around the Z resonance. The curves indicate the predicted cross-section for two, three and four neutrino species with SM couplings and negligible mass. Taken from [31].

where N_ν is the number of light ($m_\nu \leq \frac{m_Z}{2}$) active neutrinos. Figure 2.2 shows this resonance for a range of N_ν hypotheses; fitting to the data yields a value of 2.984 ± 0.008 neutrino flavours [31].

The extremely precise measurement reported by the LEP experiments was enough for many physicists to claim indisputable evidence for the existence of the tau neutrino; it was partly for this reason that its experimental discovery was not until 25 years after the addition of the τ lepton to the Standard Model. However, in 2000 the DONUT (Direct Observation of NuTau) experiment at Fermilab, IL, U.S.A. finally reported direct detection of the tau neutrino [32]. As its name suggests, DONUT was designed specifically for the purpose of finding the third neutrino. It did this by identifying the τ as the only lepton at the interaction vertex from a ν_τ beam created by firing 800 GeV protons from the Tevatron at a tungsten beam dump. The mean energy of the ν_τs detected at the emulsion target 36 m downstream

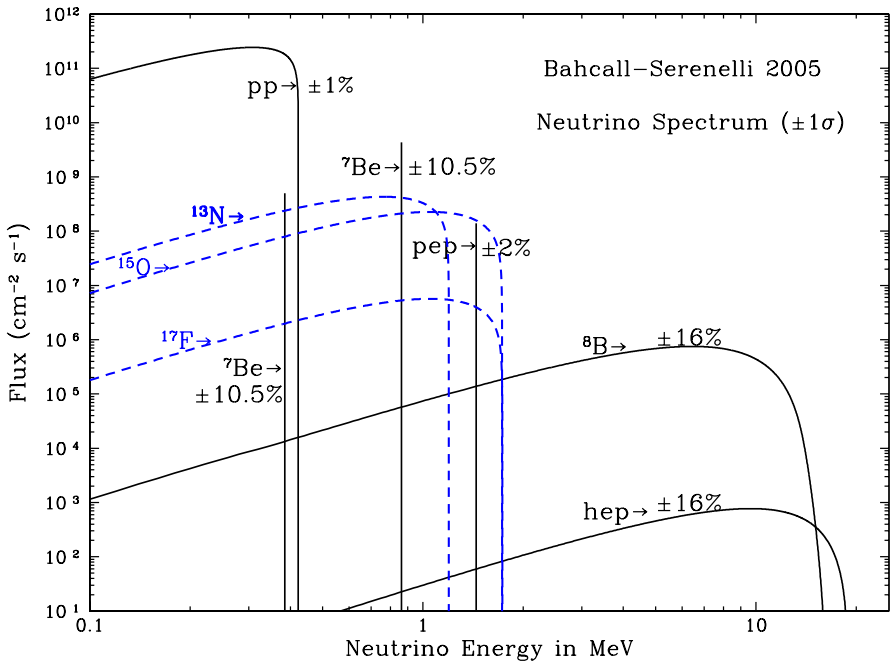

Fig. 2.3 Solar neutrino energy spectra as predicted by the Standard Solar Model [35]. The solid lines represent neutrinos produced during the p-p chain and dashed line represent neutrinos from the CNO cycle. Each spectrum illustrates a particular reaction during the process of a given chain.

was 111 GeV, produced by the decay of a D_S meson to a τ lepton and a $\bar{\nu}_\tau$ neutrino followed by the decay of the τ to a ν_τ. Four events were found, above a predicted background of 0.34 ± 0.05, consistent with the Standard Model description of the tau neutrino.

2.1.3 The Solar Neutrino Problem

It has been known since the 1930s, when Hans Bethe started developing the ideas of stellar nucleosynthesis [33], that an abundance of electron neutrinos is created as byproducts of the nuclear processes powering the Sun. The Standard Solar Model (SSM), established by John Bahcall in 1968 [34], explains the nuclear fusion processes responsible for powering stars. For stars the size of the Sun, this is dominated by the *proton-proton chain*; heavier stars follow the *CNO cycle*. Figure 2.3 shows the energy spectra of neutrinos released during reactions occurring during both chains.

Ray Davis, in collaboration with Bahcall, conducted the first experiment to detect these solar neutrinos in 1968. Using a similar detection technique to his previous experiments, Davis used a 380 m^3 tank of tetrachloroethene (C_2Cl_4) to detect neutrinos via the inverse beta decay reaction detailed in Equation 2.5. Given the threshold for this reaction is 0.814 MeV, the

main sources of neutrinos probed by this experiment were Be^7 and B^8. In order to eliminate backgrounds from cosmic rays, Davis constructed his experiment 4850 ft underground at the Homestake mine near Lead, SD, U.S.A. It is worth noting, in a pleasing neutrino-full-circle, this is exactly where the far detector for the DUNE experiment will be housed. The Davis Homestake experiment ran for 25 years but the results obtained [36] disagreed quite strongly with the SSM [37], consistently measuring solar electron neutrinos at a rate around a third of that predicted by the model. This became known as the 'solar neutrino problem', and Davis was awarded the Nobel Prize for his work on this famous experiment in 2002.

The subsequent radiochemical experiments SAGE (from 1990) and GALLEX (from 1991) were sensitive to the large flux of *pp* neutrinos by utilising a Ga^{71} target and the lower threshold reaction

$$\nu + \mathrm{Ga}^{71} \rightarrow \mathrm{Ge}^{71} + e^{-}. \tag{2.12}$$

These experiments also reported 'missing' neutrinos, determining capture rates of $66.6^{+6.8+3.8}_{-7.1-4.0}$ SNU (SAGE) [38] and $77.5 \pm 6.2^{+4.3}_{-4.7}$ SNU (GALLEX) [39], disagreeing with the SSM prediction of 130 SNU [40]. There appeared to be a problem – either the SSM was incomplete and incorrectly over-predicted the amount of electron neutrinos or hints of new physics were beginning to appear in the experiment data.

2.1.4 The Atmospheric Neutrino Anomaly

Another abundant source of natural neutrinos come from cosmic rays interacting with the upper atmosphere and producing 'atmospheric neutrinos', typically via the interactions [41]

$$\pi^{+} \rightarrow \mu^{+} + \nu_{\mu}, \qquad \mu^{-} \rightarrow e^{-} + \bar{\nu}_{e} + \nu_{\mu} \tag{2.13}$$

$$\pi^{-} \rightarrow \mu^{-} + \bar{\nu}_{\mu}, \qquad \mu^{+} \rightarrow e^{+} + \nu_{e} + \bar{\nu}_{\mu}. \tag{2.14}$$

Since the decay lengths and kinematics are well known, the predicted ratio of muon to electron neutrinos can be calculated to a good accuracy. This ratio can be compared to an experimentally determined ratio and analysed as a measure of the efficacy of the model.

It was first noticed as early as the late 1970s by experiments designed to search for nucleon decay predicted by the then-popular Grand Unified Theories that the measured flux did not correspond to that predicted by the theory. The IMB [42] and Kamioka [43] experiments, whilst measuring the atmospheric neutrino flux as an important background for nucleon decay, both noticed deficiencies in the ratio between muon and electron neutrinos compared to that predicted by the models. These experiments utilised large tanks of pure water surrounded by Photo-Multiplier Tubes (PMTs) to detect neutrinos via the Cherenkov

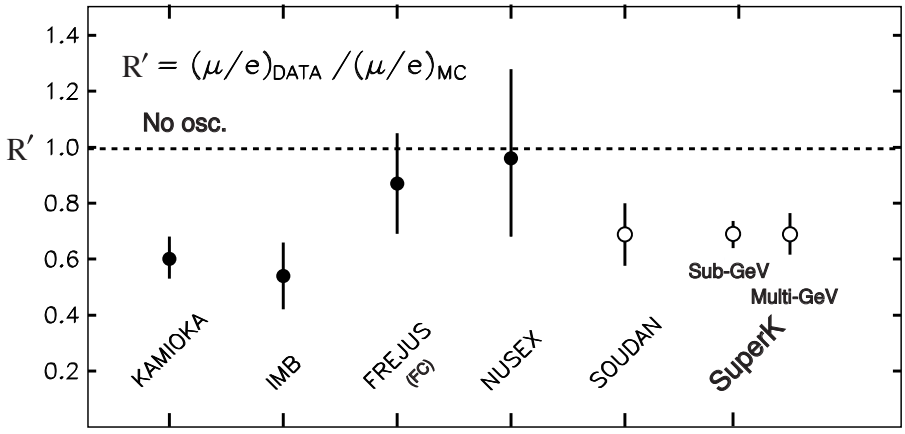

Fig. 2.4 The double ratio R of muon to electron neutrino events showing data divided by expectation [44]. Various underground atmospheric neutrino detectors are shown.

radiation created by their charged leptonic daughter particles. Using ring-imaging techniques, it is possible to distinguish between electron-like and muon-like events and therefore identify the flavour of the incoming neutrino. The problem implied by these measurements is known as the 'atmospheric neutrino anomaly'.

Various other experiments over the following twenty years also reported similar measurements, suggesting an excess of electron neutrinos over prediction, a deficit in the number of muon neutrinos, or both. Results from numerous experiments are shown in Figure 2.4. Most experiments report a discrepancy, with its size seemingly dependent on the energy region being studied. The experiments reporting a ratio consistent with one were much smaller than the others, and with more statistics they also started observing similar effects. This anomaly, along with the issue of the solar neutrino problem, strongly hinted at a problem with our understanding of neutrino physics. This is be discussed in detail in the Section 2.2.

2.2 Neutrino Oscillations

The concept of neutrino oscillations involves the changing of the flavour of a neutrino as it propagates through time and space; a neutrino created in a certain flavour has a non-zero probability of being later detected in a different flavour state. It was first postulated as an explanation of the Solar Neutrino Problem by Pontecorvo in 1968 [45, 46], having initially proposed the phenomenon in 1957 as an analogy to $K^0 \rightarrow \widetilde{K}^0$ transition in the quark sector [47]. It offers an elegant solution to both the solar neutrino problem and the atmospheric neutrino anomaly by explaining where the 'missing' neutrinos had gone; it is possible they had simply 'oscillated' to a different flavour and therefore would not be detected as expected.

2.2.1 The Evidence for Neutrino Oscillations

Whilst there was speculation that neutrino oscillations may be the explanation behind the issues observed in the data much sooner [48, 49], definite proof was not provided until the late 1990s. In many ways, the story of neutrino physics, from the initial observations of the Solar Neutrino Problem and the Atmospheric Neutrino Anomaly, through the speculation and theoretical developments, to the eventual proof, can be considered a triumph for the scientific method.

The Kamiokande and Super-Kamiokande experiments in Japan (upgrades from the Kamioka experiment noted previously) and the SNO experiment in Sudbury, Canada produced the results which showed indisputable evidence for neutrino oscillations and provided explanations for all previous discrepancies observed. This result was monumental and the work of both collaborations was rewarded in 2015 when the Nobel Prize was awarded to T. Kajita and A. McDonald, from Super-Kamiokande and SNO respectively.

2.2.1.1 Super-Kamiokande and the Atmospheric Sector

In 1994, the Kamiokande experiment produced results which hinted at an angular dependence for the R-ratio deficit, implying a dependence on neutrino travel distance [50]. This result can be explained by invoking neutrino oscillations since the probability of oscillation is influenced by the propagation distance; its significantly larger successor, Super-Kamiokande, was constructed in order to make precise measurements of this phenomenon. Super-Kamiokande is located 1000 m underground and contains an inner detector consisting of 22.5 kton fiducial volume of pure water contained within a large stainless steel cylinder (37 m high, 34 m diameter) and surrounded by 13142 20-inch photo-multipliers. With 40% coverage, the photocathodes extended over nearly an acre and provided ten times more pixels than any other experiment at the time. Its results in 1998 confirmed the earlier angular dependence findings of Kamiokande, Figure 2.5, and also considered the data as a function of neutrino energy and propagation distance, as shown in Figure 2.6. The observed effects disagreed with a view of non-oscillating atmospheric neutrinos but were entirely consistent with a two-flavour oscillation model, $\nu_\mu \rightarrow \nu_\tau$. This resulted in the famous published claim for the experimental discovery of neutrino oscillations [8].

2.2.1.2 SNO and the Solar Sector

After the Super-Kamiokande results, it was clear that neutrino oscillations would probably also explain the deficit of electron neutrinos observed by solar neutrino experiments. It took

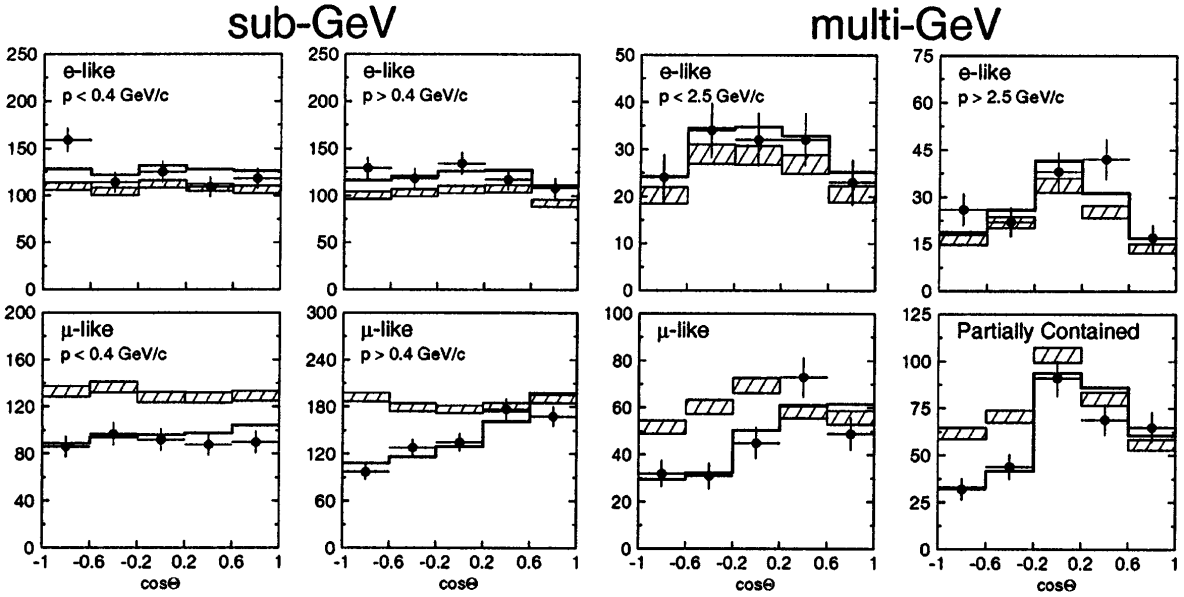

Fig. 2.5 Zenith angle distributions of μ-like and e-like events for sub-GeV and multi-GeV data sets. Upward-going particles have $\cos\Theta < 0$ and downward-going particles have $\cos\Theta > 0$. The hatched region shows the Monte Carlo expectation for no oscillations and the bold line is the best-fit expectation for $\nu_\mu \to \nu_\tau$ oscillations. Taken from [8].

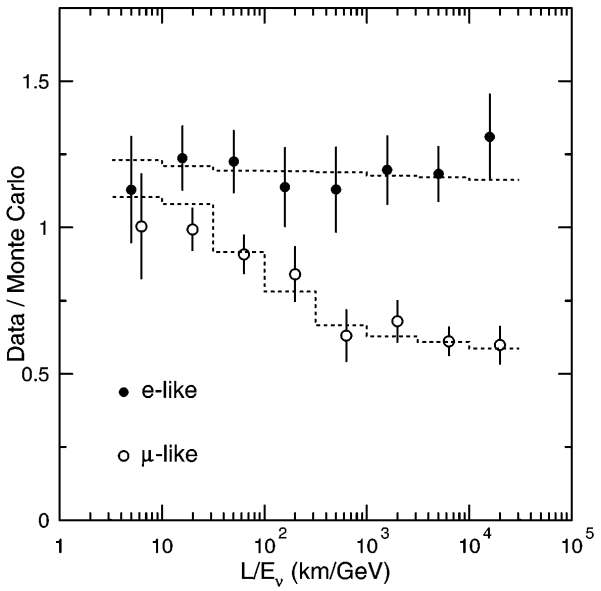

Fig. 2.6 The ratio of the number of data events to Monte Carlo events in the absence of oscillations as a function of reconstructed L/E_ν. The dashed lines show the expected shape for $\nu_\mu \to \nu_\tau$ oscillations. Taken from [8].

a few years until the Sudbury Neutrino Observatory (SNO) in Canada provided some quite brilliant evidence of this in 2002 [9].

SNO was a water Cherenkov detector, like Super-Kamiokande, but used heavy water (D_2O) as a detector medium. The water is contained in a 12 m acrylic spherical shell and surrounded by 9456 photomultipliers at a depth of 6010 m water equivalent. The use of heavy water facilitated sensitivity to other neutrino interaction channels not accessible by Super-Kamiokande via the charge current (CC), neutral current (NC) and elastic scattering (ES) interactions;

$$\nu_e + d \rightarrow p + p + e^- \qquad \text{(CC)} \tag{2.15}$$

$$\nu_x + d \rightarrow p + n + \nu_x \qquad \text{(NC)} \tag{2.16}$$

$$\nu_x + e^- \rightarrow \nu_x + e^- \qquad \text{(ES).} \tag{2.17}$$

The CC channel is sensitive exclusively to electron neutrinos, whilst the other two are accessible by neutrinos of any flavour. This allowed for the first time a simultaneous measurement of the total neutrino interaction rate as well as the electron neutrino interaction rate. The observations of SNO were the smoking gun for neutrino oscillations; the total measured flux for all neutrinos, $\phi_{\text{NC}}^{\text{SNO}} = 6.42 \pm 1.57\ (\text{stat.})^{+0.55}_{-0.58}\ (\text{sys.})\ \text{cm}^{-2}\text{s}^{-1}$, agreed excellently with the electron neutrino flux predicted by the SSM, $\phi^{\text{SSM}} = 5.05^{+1.01}_{-0.81}\ \text{cm}^{-2}\text{s}^{-1}$. However, the measured electron neutrino flux was around a third lower, $\phi_e^{\text{SNO}} = 1.76 \pm 0.05\ (\text{stat.}) \pm 0.09\ (\text{sys.})\ \text{cm}^{-2}\text{s}^{-1}$, consistent with previous measurements from the radiochemical experiments. The evidence seems conclusive: the solar models are correct and the neutrinos are not disappearing; there are simply changing their flavour state. A summary plot showing all solar neutrino experiments up until this point is depicted in Figure 2.7 [51].

2.2.2 Vacuum Oscillations

The theory of neutrino oscillations is basically the quantum mechanics of mixed states and was developed on top of Pontecorvo's work by Ziro Maki, Masami Nakagawa and Shoichi Sakata [52]. If the neutrino flavour states can spontaneously convert from one to another, none can be considered as eigenfunctions of the Hamiltonian. The true stationary states are the *mass eigenstates* (ν_1, ν_2, ν_3), of which the flavour states (ν_e, ν_μ, ν_τ) can be considered linear superpositions:

$$\begin{pmatrix} \nu_e \\ \nu_\mu \\ \nu_\tau \end{pmatrix} = U^*_{\text{PMNS}} \begin{pmatrix} \nu_1 \\ \nu_2 \\ \nu_3 \end{pmatrix}, \tag{2.18}$$

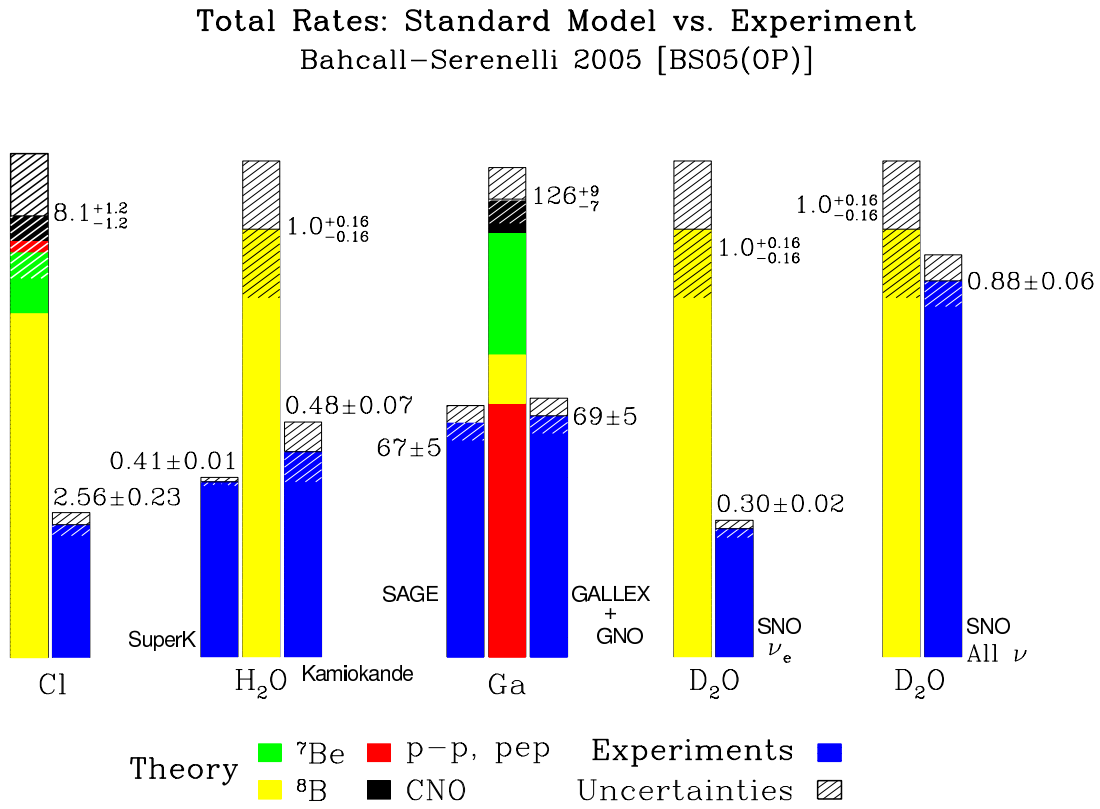

Fig. 2.7 Comparison of the predictions of the neutrino fluxes from the Standard Solar Model with measured rates from a variety of solar neutrino experiments. The results of SNO (D_2O target, right two comparisons) show that the expected flux is observed, but not necessarily as electron neutrinos. This shows conclusively the oscillatory nature of neutrinos.

where U_{PMNS} is the PMNS mixing matrix which described the flavour composition of each of the mass eigenstates, and vice versa. If the PMNS matrix were diagonal, each flavour state would correspond to a single mass state and oscillations would not occur.

Just as the flavour states are a superposition of mass states

$$|\nu_\alpha\rangle = \sum_i U^*_{\alpha i}|\nu_i\rangle, \tag{2.19}$$

the mass states can also be considered a superposition of flavour states

$$|\nu_i\rangle = \sum_\alpha U_{\alpha i}|\nu_\alpha\rangle. \tag{2.20}$$

For the three neutrino case, the PMNS matrix, decomposed into its three axial rotations, can be expressed as

$$U_{\alpha i} \equiv \underbrace{\begin{pmatrix} 1 & 0 & 0 \\ 0 & c_{23} & s_{23} \\ 0 & -s_{23} & c_{23} \end{pmatrix}}_{\text{'Atmospheric' term}} \underbrace{\begin{pmatrix} c_{13} & 0 & e^{-i\delta}s_{13} \\ 0 & 1 & 0 \\ -e^{-i\delta}s_{13} & 0 & c_{13} \end{pmatrix}}_{\text{'Accelerator' or 'Reactor' term}} \underbrace{\begin{pmatrix} c_{12} & s_{12} & 0 \\ -s_{12} & c_{12} & 0 \\ 0 & 0 & 1 \end{pmatrix}}_{\text{'Solar' term}}, \tag{2.21}$$

where $c_{ij} \equiv \cos(ij)$, $s_{ij} \equiv \sin(ij)$ and δ is a CP-violating phase factor. Each axial component is often referred to by the means with which they are studied, as shown in Equation 2.21.

The weak interaction couples to the flavour eigenstates so neutrinos are always created and detected as flavour states. However, they propagate as mass states since it is these which are eigenstates of the Hamiltonian. Due to the misalignment of the flavour and mass states, oscillations can be shown to occur. A neutrino created with flavour α is a superposition of all the mass states (Equation 2.19). These states propagate as a plane wave, evolving in time and space such that

$$|\nu_i(x,t)\rangle = |\nu_i(0)\rangle e^{-i\mathbf{x}\cdot\mathbf{p}}, \tag{2.22}$$

where $\mathbf{x}$ and $\mathbf{p}$ are the 4-position and 4-momentum of the neutrino respectively. From Equations 2.19 and 2.22, the evolution of the flavour states over space and time is therefore

$$\begin{aligned} |\nu_\alpha(x,t)\rangle &= \sum_i U^*_{\alpha i}|\nu_i(x,t)\rangle \\ &= \sum_i U^*_{\alpha i} e^{-i\mathbf{x}\cdot\mathbf{p}}|\nu_i(0)\rangle. \end{aligned} \tag{2.23}$$

In the ultra-relativistic limit, the mass of the neutrino is negligible compared to its momentum ($m_i \ll \vec{p}$) and $\vec{x} \approx ct$;

$$E_i = \sqrt{|\vec{p}|^2 + m_i^2} = \vec{p}\sqrt{1 + \frac{m_i^2}{|\vec{p}|^2}} \approx \vec{p} + \frac{m_i^2}{2\vec{p}} \tag{2.24}$$

$$\mathbf{x}\cdot\mathbf{p} = E_i t - \vec{x}\cdot\vec{p} = \vec{p}\cdot t + \frac{m_i^2}{2\vec{p}}t - \vec{x}\cdot\vec{p} \approx \frac{m_i^2}{2\vec{p}}\vec{x} = \frac{m_i^2}{2p}x, \tag{2.25}$$

assuming the neutrino displacement is in the direction of its momentum and using natural units ($c \equiv \hbar \equiv 1$). Thus, using Equations 2.23, 2.25 and 2.20,

$$\begin{aligned} |\nu_\alpha(x,t)\rangle &= \sum_i U^*_{\alpha i} e^{-i\frac{m_i^2}{2p}x} |\nu_i(0)\rangle \\ &= \sum_i \sum_\beta U^*_{\alpha i} e^{-i\frac{m_i^2}{2p}x} U_{\beta i} |\nu_\beta\rangle. \end{aligned} \tag{2.26}$$

The probability of a neutrino created in flavour state α being observed in flavour β can be determined from Equation 2.26

$$P(\alpha \to \beta) = |\langle \nu_\alpha | \nu_\beta(x,t)\rangle|^2 \tag{2.27}$$

$$= \left[\sum_i U_{\alpha i} e^{i\frac{m_i^2}{2p}x} U^*_{\beta i}\right]\left[\sum_j U^*_{\alpha j} e^{-i\frac{m_j^2}{2p}x} U_{\beta j}\right] \tag{2.28}$$

$$= \sum_{i,j} U_{\alpha i} U^*_{\alpha j} U_{\beta j} U^*_{\beta i} e^{i\frac{m_i^2 - m_j^2}{2p}x}, \tag{2.29}$$

and is observed to be dependent on the neutrino momentum, the difference between the squared masses of the flavour states, the propagation distance and the relative mixing of the two flavour states encoded in the matrix elements U.

An accelerator based neutrino experiment, such as DUNE, will typically use a ν_μ-dominated beam and look for *muon neutrino disappearance* ($P(\nu_\mu \to \nu_\mu)$) and *electron neutrino appearance* ($P(\nu_\mu \to \nu_e)$). In this case, also in the relativistic limit, the relevant appearance and disappearance probabilities can be approximated, respectively, as

$$P(\nu_\mu \to \nu_e) \approx \sin^2 2\theta_{13} \sin^2 \theta_{23} \sin^2\left(1.27\frac{\Delta m^2_{13} L}{E}\right) \tag{2.30}$$

$$P(\nu_\mu \to \nu_\mu) \approx 1 - \cos^4 \theta_{13} \sin^2 2\theta_{23} \sin^2\left(1.27\frac{\Delta m^2_{23} L}{E}\right), \tag{2.31}$$

where $\Delta m^2_{ij} \equiv m^2_i - m^2_j$ is the *mass squared splitting* in eV, L is the distance propagated in km and E is the neutrino energy in GeV.

From these equations, it can be seen the important controllable parameters relevant for observing oscillations are the neutrino energy and the distance they travel. An experiment will typically choose a ratio L/E which will attempt to maximise the effect of oscillations in order to make precision measurements.

2.2.3 Matter Effects

The oscillations considered thus far are *vacuum oscillations* which occur due to the mixing of the neutrino mass and flavour states. Whilst directly confirming the oscillation of solar neutrinos, the SNO experiment (along with every other solar neutrino experiment) reported more oscillations than can be explained using just the vacuum oscillation model discussed in Section 2.2.2 [53, 54]. When neutrinos propagate through matter, an additional potential can be shown to also produce oscillations, which would occur even in the case of massless neutrinos (as long as mixing occurs). Since solar neutrinos travel through dense matter before exiting the Sun, it is possible these matter effects explained above could explain this discrepancy.

Coherent scattering (scattering in which the neutrino state is unchanged) due to interactions with the medium cause neutrinos travelling through matter to feel a potential. As normal matter is composed of electrons, rather than their heavier counterparts muons and taus, electron neutrinos are affected more by this potential. The mechanism for this is demonstrated in Figure 2.8. This gives rise to an additional effective mass splitting between the electron neutrino and the other flavours and therefore results in the possibility of oscillations [55]. Due to the density of the Sun and the neutrino energies, the neutrinos actually feel a resonance which causes their oscillation probability to become dramatically higher than the vacuum oscillation probabilities. This is known as the Mikheev-Smirnov-Wolfenstein (MSW) effect [56, 57]. It is worth pointing out at this point that, since normal matter is composed of electrons and not positrons, this effect is also different for ν_es and $\bar{\nu}_e$s; the importance of this becomes apparent when considering the additional effects of CP-violation.

2.2.3.1 KamLAND and Reactor Neutrinos

In order to investigate the possible MSW effects in the Sun, measurements of electron neutrino disappearance from terrestrial neutrinos, which were not subject to these matter effects, were considered. The first experiment to publish results was KamLAND (Kamioka Liquid Scintillator Anti-Neutrino Detector) in 2003 [58, 59]. KamLAND occupied the site

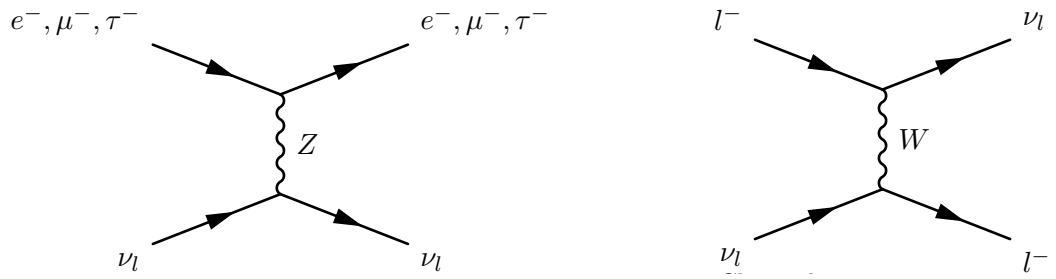

(a) Neutral current scattering.

(b) Charged current scattering.

Fig. 2.8 General scattering mechanics which occur as neutrinos pass through matter. Neutral current scattering (Figure 2.8a) occurs for all neutrino flavour combinations whereas charged current scattering (Figure 2.8b) only occurs when the incoming leptons have the same flavour.

previously used by the Kamiokande experiment in Japan under 2700 m.w.e of rock and utilised 1 kton of ultra-pure liquid scintillator contained in a 13 m spherical balloon. It was surrounded by 53 Japanese nuclear power reactors with baselines ranging from 80 km to 800 km and detected the $\bar{\nu}_e$s via the inverse beta decay reaction $\bar{\nu}_e + p \rightarrow e^+ + n$. Scintillation light from the delayed coincidence of a positron with the neutron capture was detected using 1879 PMTs and constituted a signal with very low background. The results from KamLAND confirmed the apparently large matter effect in solar neutrinos and completely solved for the first time the long-standing Solar Neutrino Problem [60–62].

2.2.4 CP-Violation

The δ terms in Equation 2.21 are CP-violating phase factors. They could be included in any of the diagonalised components but are generally added to the accelerator part since this is how current and future experiments will look for evidence of CP-violation. As long as all the mixing angles are non-zero, there is the possibility of CP-violation in the lepton sector.

This is an exciting prospect and one of the reasons for the current intense interest in neutrino physics. It is known CP-violating processes must have occurred in the early Universe since matter has come to dominate massively over antimatter after they were created equally in the Big Bang. This has been observed in the quark sector but current experimental evidence can only account for a small amount of the necessary CP-violation. It is also expected but has never been observed in strong interactions [63]. Leptonic CP-violation could potentially account for the matter-antimatter asymmetry in the Universe and ultimately explain how it evolved to include our very existence [64, 65].

In neutrino experiments, effects of CP-violation would be apparent as a difference in behaviour between neutrinos and antineutrinos. For example, since the sign of δ is different

for neutrinos and antineutrinos, an asymmetry

$$\mathscr{A} = \frac{P(\nu_\mu \to \nu_e) - P(\bar{\nu}_\mu \to \bar{\nu}_e)}{P(\nu_\mu \to \nu_e) + P(\bar{\nu}_\mu \to \bar{\nu}_e)} \tag{2.32}$$

can be observed and measured.

2.3 Status of Neutrino Physics

The field of neutrino physics has advanced rapidly over the past twenty to thirty years (discussed in Sections 2.1 and 2.2) and there is currently a good understanding of most experimental results in the context of 3-flavour neutrino oscillations. Presently, the focus has shifted to making precise measurements of the oscillation parameters and trying to understand the nature of neutrino mass. The current understanding of each of these areas will be presented in Sections 2.3.2 and 2.3.3 respectively following a brief overview of current and future experiments in Section 2.3.1.

2.3.1 Current and Future Experiments

In recent years, neutrino experiments which utilise a custom built artificial neutrino beam have been offering complimentary and world-leading results. These 'accelerator experiments' are used in order to have more control over the energy spectrum and composition of the neutrino beam and often use a long-baseline, sampling the beam at different points to determine the effects of oscillation as the neutrinos propagate in between.

MINOS was based at Fermilab, U.S., and detected neutrinos from the NuMI (Neutrinos at the Main Injector) beam at a 'near detector' and then again in Northern Minnesota, a baseline of 735 km. T2K follows a similar design and uses the Super-Kamiokande detector as the far detector, utilising a beam from J-PARC, Japan and a baseline of 295 km. T2K and NOνA, another current long-baseline experiment, were designed specifically to measure the last mixing parameter, θ_{13}, by looking for ν_e appearance in a ν_μ beam. NOνA, like its predecessor MINOS, also uses the NuMI beam and has a far detector at the same site. However, along with T2K, it is 'off-axis' by around 2°; this produces a more monotonic neutrino energy spectrum to maximise the effect of oscillations and make more accurate measurements. T2K and NOνA still have many years left of their respective programmes and are currently making precision measurements of the mixing parameters along with constraining CP-violation by combining neutrino and antineutrino analyses. They will not be

able to make statistically significant measurements of this area but, especially through joint analyses, will be able to offer hints before the next generation of experiments.

Future long-baseline experiments include DUNE [66], which will be discussed properly in Chapter 3, and Hyper-Kamiokande [67], an upgrade of the current T2K experiment. Hyper-Kamiokande will also use water Cherenkov technology but will boast a fiducial volume 25 times larger than that of Super-Kamiokande. The timescale of these projects is on the order of at least ten years from now and both pose incredible engineering challenges in their own right.

2.3.2 Oscillation Parameters

The current status of the mixing angles and the mass-squared differences is depicted in Figure 2.9. The world-best measurements for θ_{12} and Δm^2_{12} are provided by the solar neutrino experiments (Homestake [36], GALLEX [68], SAGE [69] and SNO [70]) and KamLAND [71]. The leading measurements in the atmospheric neutrino sector, θ_{23} and $|\Delta m^2_{32}|$, are from Super-Kamiokande [72], IceCube [73] and the accelerator experiments MINOS [74, 75], T2K [76] and NOνA [77].

The value of θ_{13} was known, from limits determined from global fits to world data, to be much smaller than the others and was even consistent with zero. In addition to the accelerator experiments, reactor neutrino experiments are also sensitive to θ_{13} via $\bar{\nu}_e$ disappearance and it was these experiments which produced the decisive results first. Daya Bay [80] in China and RENO [81] in South Korea found evidence of a non-zero value in 2012. There is good agreement between these reactor experiments and more recent measurements from T2K [82] and NOνA [83].

A summary of the best known values for all these oscillation parameters is shown in Table 2.1. The CP-violating phase δ_{CP} is currently unmeasured and provides a priority for current and future neutrino experiments. T2K have excluded the CP conservation regions with little statistical significance and currently favours a maximal CP-violation value of $\delta_{\text{CP}} = -\pi/2$ [84] [NOTE TO ME! Just preprint, may be published by the time I've finished writing this thing!]; this holds much promise for future experiments. The octant of θ_{23}, the location of the parameter in either the $> 45^\circ$ or $< 45^\circ$ octant, is also undetermined and requires high precision measurements; it is possible that the mixing in this sector is 'maximal' ($\theta_{23} = 45^\circ$).

2.3.3 Neutrino Mass

Neutrinos in the Standard Model are massless, for no real reason. However, the observation of neutrino oscillations implies the existence of neutrino mass (the oscillation probabilities,

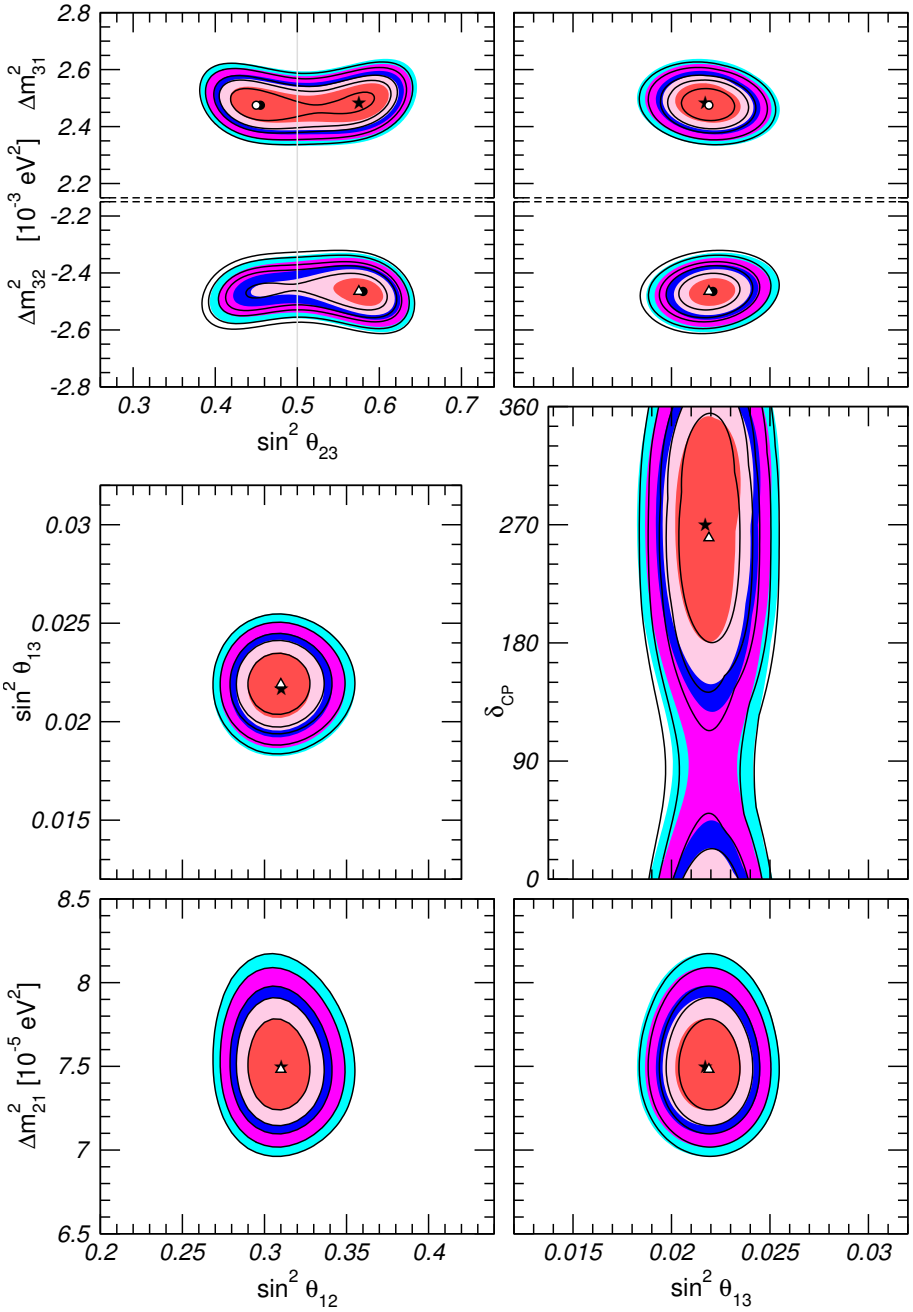

Fig. 2.9 Global 3-neutrino oscillation analysis taken from [78, 79]. Each panel shows the two-dimensional projection of the allowed six-dimensional region after marginalisation with respect to the undisplayed parameters. The different contours correspond to 1σ, 90%, 2σ, 99%, 3σ CL (2 dof).

Table 2.1 The current best-fit values for the neutrino oscillation parameters for normal (inverted) hierarchy. Taken from [79].

Parameter	Best fit ($\pm 1\sigma$)
$\sin^2\theta_{12}$	0.306 ± 0.012
$\sin^2\theta_{23}$	$0.441^{+0.027}_{-0.021}$ ($0.587^{+0.020}_{-0.024}$)
$\sin^2\theta_{13}$	0.02166 ± 0.00075 (0.02179 ± 0.00076)
Δm^2_{12} [10^{-5} eV^2]	$+7.50^{+0.19}_{-0.17}$
$\lvert\Delta m^2_{3\nu}\rvert$ [10^{-3} eV^2]	$2.524^{+0.039}_{-0.040}$ ($-2.514^{+0.038}_{-0.041}$)
δ_{CP} [$^\circ$]	261^{+51}_{-59} (277^{+40}_{-46})

such as Equations 2.30 and 2.31, would be zero if there was no mass splitting). Three active neutrino flavours gives rise to two independent mass splittings, Δm^2_{12} and Δm^2_{32}, as appear in the oscillation probabilities. Unfortunately, fitting to the oscillation results provides only a handle on the value of these splittings and not the signs, resulting in an ambiguity in the ordering of the mass states. This can be resolved in the solar sector by utilising the effect of the MSW resonance encountered by neutrinos in the Sun, allowing the sign of Δm^2_{12} to be known (it must be positive as otherwise fewer oscillations, not more, will have been observed by SNO and the other solar neutrino experiments). This leaves two possible 'hierarchies', normal and inverted, which are possible given the experimental data. These mass splittings also do not offer any indication of an absolute mass scale for the neutrino mass states, this must be constrained using other methods and is currently undetermined. These uncertainties are illustrated in Figure 2.10.

DUNE will use the MSW effect present as neutrinos propagate through the Earth's crust in order to resolve the hierarchy problem. It is essential that the hierarchy is resolved since the associated asymmetries between neutrinos and antineutrinos can mimic true CP-violation, which therefore cannot be measured accurately until the mass splittings are completely understood. Due to the large matter effects associated with its long baseline, the NOνA experiment is sensitive to the mass hierarchy and may be able to have a say before DUNE and Hyper-Kamiokande.

The absolute neutrino mass cannot be measured from oscillation experiments so other techniques have been developed. It is possible to use information from β-decay to get a handle on the mass scale; the $\bar{\nu}_e$ mass alters the spectrum of electrons near the end point so precision measurements can study this effect. The current best limits on the mass are from H^3 β-decay experiments and yield $m_{\bar{\nu}_e} < 2.05$ eV at 95% C.L. [85, 86]. Cosmological analysis can also constrain the absolute neutrino mass by looking at the distribution of matter

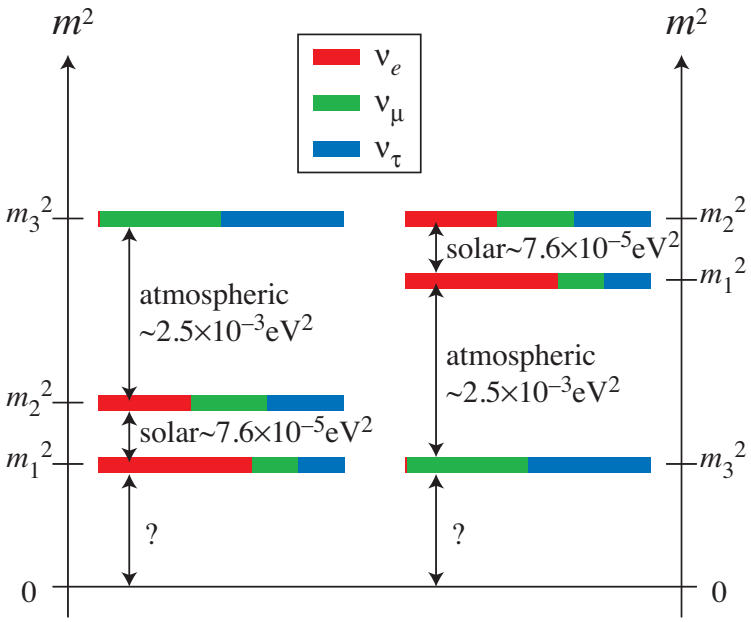

Fig. 2.10 Demonstration of the current uncertainties in the neutrino mass. The undetermined sign in the mass splitting between the 2 and 3 states leaves two possible 'hierarchies' open: normal (left figure) and inverted (right figure). The absolute scale of the masses is also currently unknown. The flavour composition of each of the mass states, given by the mixing angles, is denoted by the coloured bars.

in the Universe and information such as galaxy clustering. The Planck collaboration reported the upper limit on the sum of all neutrino masses as $\sum_i m_{\nu_i} < 0.23$ eV at 95% C.L. in 2013 [87], indicating a significantly lower mass scale than is attainable using current experiments.

Chapter 3

The Deep Underground Neutrino Experiment

The Deep Underground Neutrino Experiment (DUNE) experiment [66, 88–90] is a future long-baseline neutrino experiment with a diverse physics program hosted by Fermilab, IL, U.S.. The far detector will be at the Sanford Underground Research Facility (SURF) near Lead, South Dakota, providing a baseline of 1300 km. A cartoon of the experiment is shown in Figure 3.1.

The DUNE experiment will be discussed in this present chapter. As the experiment utilises liquid argon TPCs, a brief history and description of this detector technology is provided as a basis in Section 3.1. An overview of the experiment, including its motivation, will be presented in Section 3.2 before the experimental details are discussed in Section 3.3. The sensitivities of the experiment and its potential discoveries are the subject of Section 3.4. Finally, the schedule and stategy implemented by the collaboration to ensure commencement of data taking in around ten years' time is outlined in Section 3.5.

3.1 The LAr TPC Concept

The use of a liquid argon time projection chamber (LArTPC) as a high-precision fine-grained detector medium holds much promise for the successful resolution of the open questions in neutrino physics. A great amount of R&D work has taken place to advance the maturity of the technology and pioneering experiments, such as ICARUS [91], have further increased the understanding of the neutrino community of the detector techniques. Past and currently running experiments at Fermilab, such as ArgoNeuT [92], LArIAT [93] and MicroBooNE

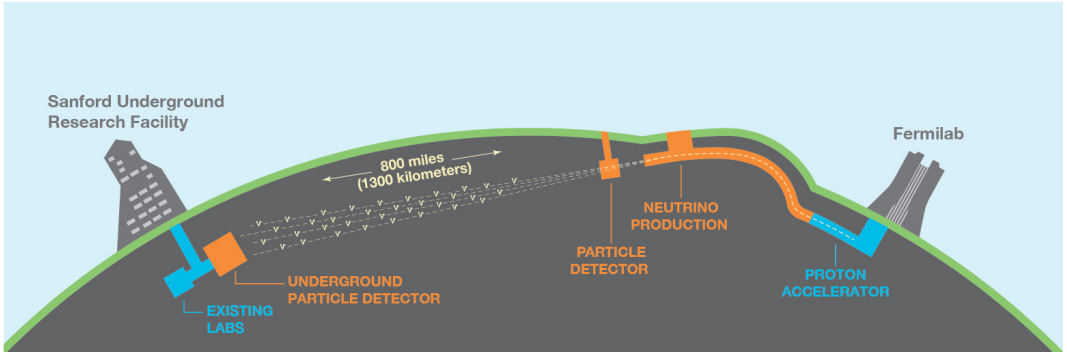

Fig. 3.1 Cartoon showing the configuratuon of the Deep Underground Neutrino Experiment. The experiment will be based at Fermilab, shown at the right of the figure, and will send neutrinos towards SURF, at the left hand side. The distance travelled, through the Earth's crust, will be 1300 km.

[94], are successfully using LArTPCs to take and analyse data and it seems certain to be the future of neutrino physics in the U.S. [95].

This section will provide a brief history of LArTPC technology and motivate its potential when used in a large experiment such as DUNE. The basic operation of such a detector will also be described to provide background for discussion of the DUNE and 35 ton experiments, and of reconstruction in LArTPCs, in future chapters.

3.1.1 A Brief History of Time (Projection Chambers)

The use of a time projection chamber as a potential particle detector was put forward by David Nygren in 1974 [96]. He envisioned bubble-chamber quality data but with the possibility of digital readout of the data, facilitating extremely fine spatial resolution, good timing resolution and fast recovery after triggering. The basic concept is a drift chamber containing a noble gas placed within a field to drift ionisation electrons created by a propagating particle towards a multielectron array. This setup allows full three-dimensional reconstruction by combining information from the two-dimensional readout plane with the drift time. Nygren also included a magnetic field to assist particle identification in his design, shown in Figure 3.2.

The extension of this concept to a liquid argon TPC and its potential as a high-precision fine-grained detector medium in neutrino physics was proposed by Carlo Rubbia in 1977 [97]. The use of a noble liquid rather than gas is necessary in neutrino experiments to provide a high enough target mass for increased probability of neutrino interactions. Noble liquids have high electron mobility and low diffusion, favourable properties as the detection of particles is from the ionisation and scintillation light created by the particles. Given the necessity of a high electric field in order to drift these electrons to the readout places, excellent dielectric

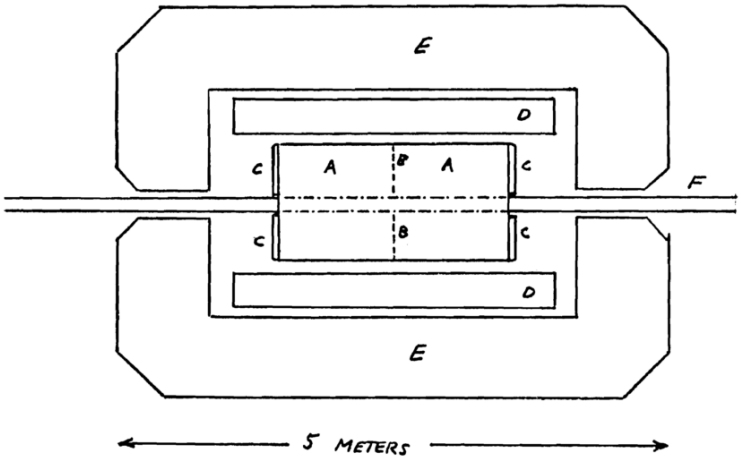

Fig. 3.2 The original concept of the time projection chamber particle detector, drawn by David Nygren in 1974 [96]. The sections are labelled as followed: methane-filled region (A), screen to establish electron field (B), end-cap detectors (C), superconducting solenoid (3.33 T) (D), iron return yoke for magnetic field (E), beam vacuum pipe (F).

properties are also required; noble liquids possess such qualities. The properties of liquid argon which make it almost perfect for this use are demonstrated in Table 3.1.

An additional advantage of this technology is the low threshold for detection; this is set by the ionisation threshold of liquid argon and is only 23.6 ± 0.5 eV [99]. Rubbia realised that a LArTPC could be the digital replacement for the high quality particle detection methods used in bubble chambers, very common in neutrino physics in the 1970s. He proposed the first LArTPC detector design, shown in Figure 3.3, which bears a striking resemblance to the LArTPCs in use today.

Table 3.1 Properties of noble liquids relevant when considering a TPC medium for a neutrino experiment [98].

	Water	He	Ne	Ar	Kr	Xe
Boiling point [K] @ 1 atm	373	4.2	27.1	87.3	120.0	165.0
Density [g/cm^3]	1	0.125	1.2	1.4	2.4	3.0
Radiation length [cm]	36.1	755.2	24.0	14.0	4.9	2.8
Scintillation [γ/MeV]	-	19 000	30 000	40 000	25 000	42 000
dE/dx [MeV/cm]	1.9	0.24	1.4	2.1	3.0	3.8
Scintillation λ [nm]	-	80	78	128	150	175
Natural abundance (Earth atm) [ppm]	5×10^4	5.2	18.2	9340.0	1.10	0.09
Electron mobility [cm^2/Vs]	low	low	low	400	1200	2200

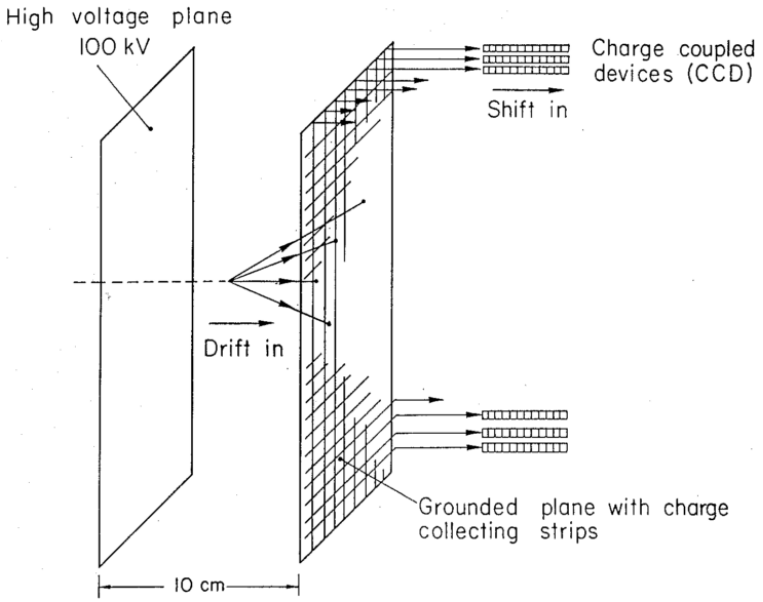

Fig. 3.3 The LArTPC detector proposed by Carlo Rubbia in 1977 [97].

Constructing and operating such a detector was beyond the technology of the time, and is still being understood today. The operation of a LArTPC detector and the challenges associated with this are the subject of Section 3.1.2.

3.1.2 LAr TPC Operation

A LArTPC typically consists of one or more anodes and cathodes at either end of an active drift region. An ionising particle passing through a LArTPC causes electrons to become free from argon atoms and, in the presence of a field, drift towards an anode where they are read out.

The readout consists of multiple wire planes with different orientations to facilitate the reconstruction. The wires are either ‘induction’ wires, which allow the electrons to deposit charge but continue past, or ‘collection’ wires, on which the electric field lines end and all the charge on the electron is collected. Each wire plane is therefore held at a different ‘bias voltage’ to prevent any field lines ending on the induction wire, thus creating local electric fields which promote the continuing forward motion of the electrons. The signal seen is therefore dependent on the type of wire plane; a bipolar pulse on an induction plane wire and unipolar on a collection plane wire. It is also common, though not essential, to make use of a ‘grid plane’ upstream of the signal planes in order to shield them from the electron charge until the drift electrons are close. Without such a plane, the bipolar pulse would be highly asymmetric, though would still have zero integral. It also makes changing the drift voltage

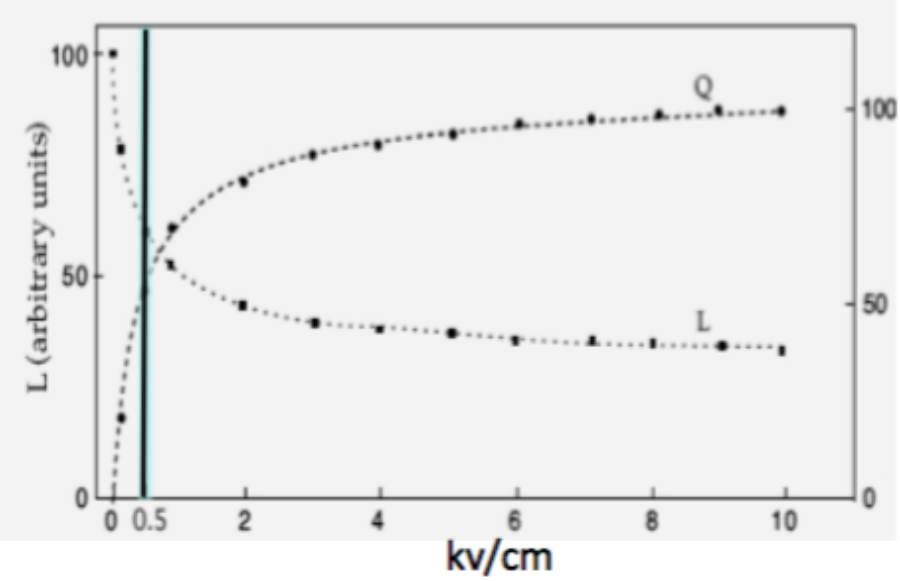

Fig. 3.4 Demonstration of the competing effect the electric field has on the luminosity of the ionisation electrons and scintillation light arriving at the detector readout. Since both are essential in reconstructing the complete interactions, a balance must be found. [PLACEHOLDER IMAGE].

(controlling the electric field) slightly easier as the signal planes are somewhat shielded from its effects. MicroBooNE does not operate with a grid plane and, although the 35 ton and the DUNE reference design make use of a grid plane, it is uncertain whether the benefit outweighs the cost for a huge LArTPC detector such as the DUNE far detector. There are alternative readout possibilities to this typical design which have been suggested but, given the scale of future LArTPCs, it is highly unlikely a viable solution which delivers superior readout at a comparable cost will be found.

Upon ionisation, an electron has a certain probability (around 60%) of recombining before the field can separate it from its ion. Whilst this compromises the signal observed, it is accompanied by a flash of scintillation light which may be detected and used to assign an 'event time' to the interaction, known as T0. Without this information, it would be impossible to place an absolute time scale on the event and result in an unresolved coordinate along the drift direction. The magnitude of the applied electric field must be chosen to balance these two effects; a larger field would result in less recombination and therefore compromise the scintillation light while a smaller field would have consequences on the signal received at the wire planes. Figure 3.4 demonstrates this and justifies the field value of 500 V/cm which is often chosen in current LAr neutrino experiments.

The basic operational principles of a LArTPC is demonstrated in Figure 3.5. The specifics of how the ionisation charge and the scintillation light is collected and processed is experiment-specific and will be discussed in the context of DUNE in Chapter 3 and the 35 ton experiment in Chapter 4. This information is all that is required to fully understand and analyse the interactions occurring in the detector; methods used to reconstruct particles and interactions in LAr will be the subject of Chapter 5.

3.1.3 LArTPC Challenges

There is no doubt of the promise of LArTPCs for the future of neutrino physics but with such expectation comes many challenges. This will be elaborated upon in more detail when discussing the 35 ton run in Section 4.8 but will be briefly mentioned here for completeness.

Given the drift fields required, and the necessary distances, the associated high voltage on the cathode must be on the order of $\sim$100 kV. This presents engineering challenges related to the feedthrough and cryostat design but also can lead to dielectric breakdown of the liquid nearby such huge voltages. The properties of LAr and the design implications must be very well understood to ensure this does not endanger the quality of the detector medium.

The presence of electro-negative impurities in the argon can capture drift electrons as they travel towards the anode planes and hinder the signal observed. The probability of this recombination is referred to as the 'electron lifetime' and is directly affected by the maintained purity of the argon. DUNE expects a contaminant no greater than ## ppm O2 and ## ppm N2 [to be filled in when I write the DUNE chapter]. This necessitates a purification system to remove impurities and requires the constant recirculation of the liquid through it. A liquifier is also necessary to recondense any boiled-off gases at the surface.

Along with the possibility of lost signal through finite electron lifetimes, the electrons may also undergo interactions and drift off course either transversely or longitudinally. This 'diffusion' affects the location and size of the observed signal so must also be well understood.

With so much resting on the success of the DUNE experiment, and considering all these effects which must be understood, prototyping is essential. The 35 ton prototype was constructed as an attempt to better understand LArTPCs and is the subject of Chapter 4.

3.2 Overview of DUNE

The outstanding questions in neutrino physics discussed in Section 2.3, namely the resolution of the mass hierachy, the determination of the CP-violating phase δ_{CP}, the measurement of the octant of θ_{23} and precision calculations of all the mixing angles, motivate the need for

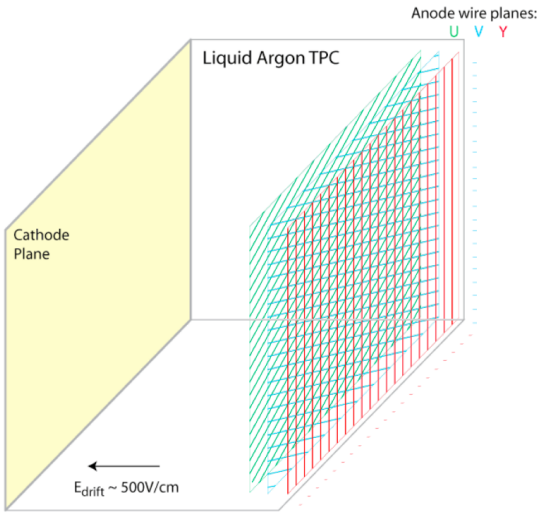

(a) Typical LArTPC with one cathode (left) and three read out anode planes (right) (two induction, U and V, and one collection, Y), setting up an electric field. The central region is filled with liquid argon.

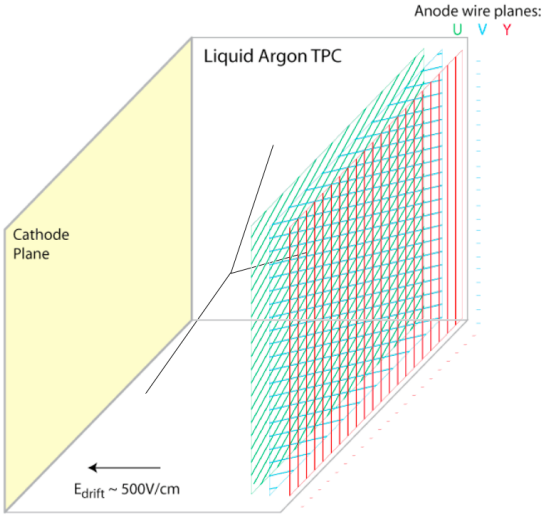

(b) An ionising particle enters the detector and liberates electrons from the medium, which then drift towards the anode planes.

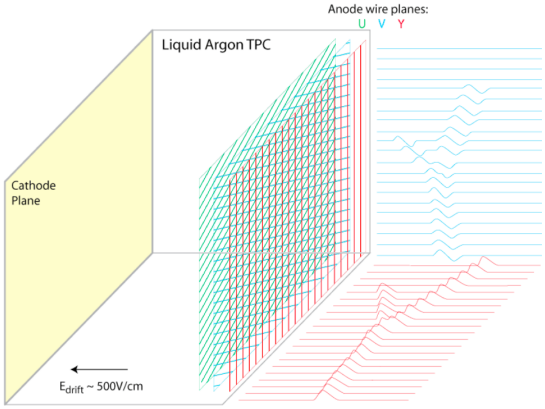

(c) As the electrons drift through, charge is induced on the first two wire planes and collected on the final one. Due to the differing orientations of the wires between planes, three complementary views of the interaction are provided (two are shown).

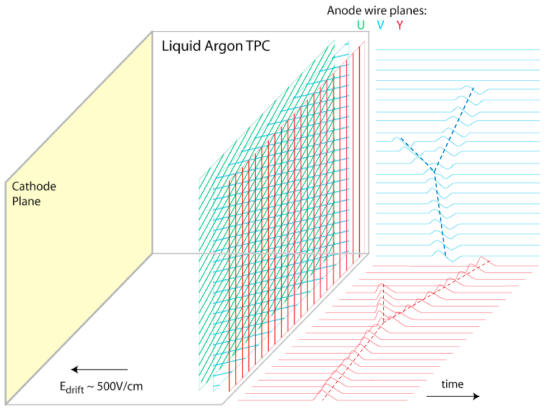

(d) By combining the two dimensional information provided by the anode planes with the drift time information, the original particle tracks can be inferred.

Fig. 3.5 Schematic demonstrating the basic operational principles of a LArTPC. The images are stills taken from an illustration created by Bo Yu (BNL) (do I need to cite this? It's a very common slide and I can't actually find a Bo Yu talk with it in... everyone just puts his name on the slide!).

next generation experiments. The DUNE experiment will make decisive contributions to each of these areas; it will also search for nucleon decay with the ability to set world-leading proton lifetime limits and make detailed, unique measurements of the ν_e flux from a core-collapse supernovae within our galaxy should one occur during the experiment. Along with this, DUNE will be used to look for Beyond Standard Model physics (such as non-standard interaction and sterile neutrinos), signatures of dark matter and, utilising the capable near detector, measurements of a range of neutrino cross-sections and nuclear effects including final state interations.

The chosen technology for the DUNE far detector, in order to maximise sensitivity to all these factors, is a liquid argon (LAr) TPC (LArTPC), introduced and described in Section 3.1. The detector will contain four modules, each comprised of 10 kt fiducial LAr and separate data acquisition and readout systems. The beam will be provided by Fermilab as part of its PIP-II program [100] and will be wide band, enabling the study of a range of neutrino energies. This facilitates a study of multiple oscillation peaks, essentially due to differing L/E ratios, and is relevant when considering the effects of an unknown CP-violating phase and unresolved mass hierarchy. Since the impact of both of these uncertainties is apparent as an asymmetry between neutrinos and antineutrinos (Equation 2.32), there is an implicit degeneracy which must be resolved to ensure both phenomena are correctly determined. Having access to multiple oscillation peaks means this may be dealt with in a single experiment, as demonstrated in Figure 3.6 [101].

DUNE was officially formed in early 2015 following the dissolution and merging of two leading next generation long-baseline experiments: the Long Baseline Neutrino Experiment (LBNE) in the U.S. [102–104] and the Large Apparatus for Grand Unification, Neutrino Astrophysics, and Long Baseline Neutrino Oscillations (LAGUNA-LBNO) in Europe [105]. Given the scale of these projects, it was decided in 2014 that efforts should be focussed on one flagship experiment utilising the expertise of as many experts in neutrino physics and LArTPC technology as possible [106]. The Particle Physics Project Prioritisation Panel review recommended..... The benchmark DUNE design is very similar to that of the former LBNE experiment, which also made use of an upgraded Fermilab neutrino beam and a large LArTPC at SURF, and gained the understanding of dual phase LArTPC detectors developed by LAGUNA-LBNO. Need to mention dual phase in the first section. It is likely that at least one of the four DUNE detector modules will be a dual phase LArTPC.

The experiment will be facilitated by the Long Baseline Neutrino Facility (LBNF), which will oversee the technical side of the project and ensure the DUNE experiment can function as desired. The relationship between the LBNF and the DUNE projects is based on the model used at CERN to manage the Large Hadron Collider (LHC) and each of the experiments

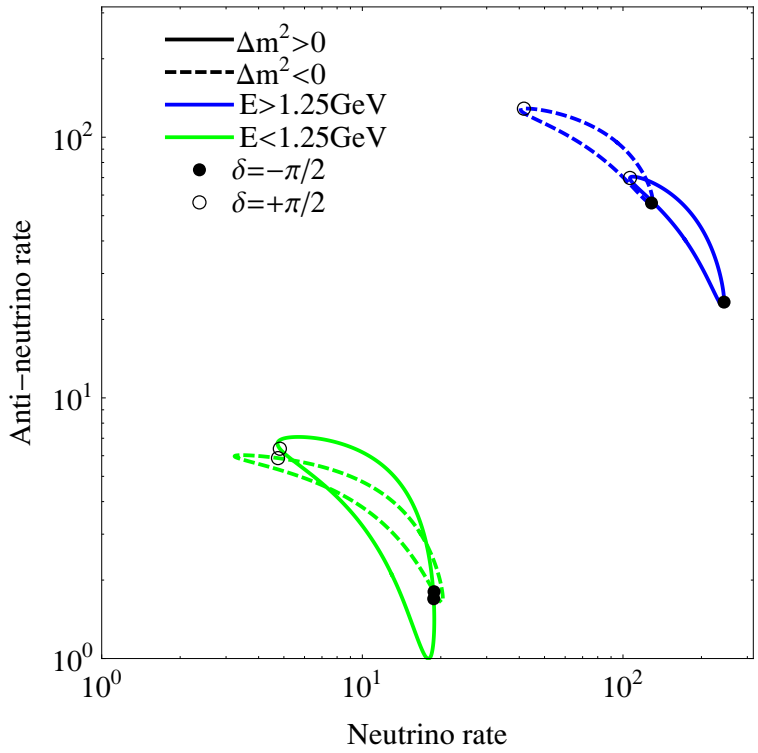

Fig. 3.6 Demonstration of how having access to multiple oscillation maxima facilitates measurements of both the neutrino mass hierarchy and leptonic CP-violation using the same experiment. In the plot, θ_{13} is held constant and the rates are determined by the number of neutrino and antineutrino events respectively. Assuming a baseline of 1300 km, as for DUNE, the first oscillation maximum is at $E_\nu = 2.5$ GeV and the second is at $E_\nu = 0.84$ GeV. The banana-shaped distributions are obtained as the value of δ_{CP} is varied from $-\pi$ to π. There is good separation between the distributions associated with each hierarchy at the first maximum whereas at the second maximum this is degenerate and the rates are similar for a given value of δ_{CP} regardless of the hierarchy. It can be seen how complimentary measurements at each maxima can be used to make unambiguous measurements of both the mass hierarchy and of CP-violation with the same experiment. Taken from [101].

which use it. LBNF has its own management structure and operates separately from DUNE, though the two projects work closely together. It is supported mainly via the Department of Energy in the U.S. whereas DUNE is internationally funded. The DUNE collaboration is responsible for defining the scientific goals of the experiment and the corresponding techincal requirements. Using these, LBNF will design and construct all technical facilities, such as the beam upgrade, the facilities for the near detectors at Fermilab and the excavation and outfitting of the large caverns for the far detectors underground at SURF along the required infrastructure to support the construction of the cryostats and the required cryogenic systems. DUNE will provide the four massive LArTPCs and the near detector systems, to be constructed at the sites supplied by LBNF. These will be discussed further in Section 3.3. During the lifetime of the experiment, LBNF is responsible for the maintaining and operation of all the facilities whilst DUNE will commission and operate the detectors. The scientific research program conducted with the collected data is the duty of the DUNE collaboration and will be explored in Section 3.4.

Given the scale of the projects, work is already underway. Construction at the far detector site starts this year, with installation of the first detector module due to commence in 2021. The start of the DUNE experiment will then correspond to the completion of this module, scheduled in 2014. The PIP-II upgraded 1.2 MW beam will be ready in 2025 and will signify the commencement of beam data taking. Subsequent detector modules will be added as soon as is feasible thereafter, increasing the fiducial volume up to the target mass of 40 kt. Further beam upgrades, up to 2.4 MW (PIP-III) are envisaged beyond this to bring the experiment up to full power and maximise the physics capability of the project. The timescales of both the LBNF and DUNE projects, along with all the essential research which must be conducted as the plans progress, is the subject of Section 3.5.

3.3 Experimental Details

3.3.1 Beam

3.3.2 Near Detector

3.3.3 Far Detector

3.4 The DUNE Effect

The staged approach to the DUNE experiment will allow early preliminary results but will require more time for facilities from later phases to be constructed and commissioned. For

Table 3.2 Exposures anticipated for the DUNE experiment for the first few years of operation. Due to the staged approach in construction, it will take a few year to reach full design capabilities. The first exposure column represents the exposure expected in that year and the next column the cumulative total.

Year	Exposure (kt·MW·year)	Total (kt·MW·year)	Detector stage
Year 1	10.7	10.7	10 kt far detector, no near detector, 1.07 MW 80 GeV proton beam (1.47×10^{21} pot per year)
Year 2	21.4	32.1	Addition of second 10 kt far detector module
Year 3	32.1	64.2	Addition of third 10 kt far detector module and initial constraints from near detector
Year 4	42.8	107.0	Addition of fourth 10 kt far detector module
Year 5	42.8	149.8	Inclusion of constraints from full near detector data analysis
Year 7	85.6	278.2	Upgrate beam power to 2.14 MW for 80 GeV proton beam

this and other reasons, the accumulated data is often referred to as an ‘exposure’, a function of detector size, beam power and time with units kt·MW·year. The current assumptions on exposures for the first few years of operature are shown in Table 3.2.

3.5 The Road to DUNE

References

[1] Sheldon L Glashow. Partial-symmetries of weak interactions. *Nuclear Physics*, 22(4):579–588, 1961.

[2] Steven Weinberg. A Model of Leptons. *Phys. Rev. Lett.*, 19(21):1264–1266, 1967.

[3] G. Aad, et al. Observation of a new particle in the search for the Standard Model Higgs boson with the ATLAS detector at the LHC. *Physics Letters B*, 716(1):1–29, 2012.

[4] S. Chatrchyan, et al. Observation of a new boson at a mass of 125 GeV with the CMS experiment at the LHC. *Physics Letters, Section B: Nuclear, Elementary Particle and High-Energy Physics*, 716(1):30–61, 2012.

[5] Tara Shears. The Standard Model. *Phil. Trans. Roy. Soc. Lond.*, A370:805–817, 2012.

[6] S M Bilenky. Neutrino in standard model and beyond. *Physics of Particles and Nuclei*, 46(4):475–496, 2015.

[7] John Ellis. Outstanding questions: Physics beyond the Standard Model. *Phil. Trans. Roy. Soc. Lond.*, A370:818–830, 2012.

[8] Y Fukuda, et al. Evidence for Oscillation of Atmospheric Neutrinos. *Phys. Rev. Lett.*, 81(8):1562–1567, 1998.

[9] Q R Ahmad, et al. Direct Evidence for Neutrino Flavor Transformation from Neutral-Current Interactions in the Sudbury Neutrino Observatory. *Phys. Rev. Lett.*, 89(1):11301, 2002.

[10] Wolfgang Pauli. Open letter to the participants of the conference in Tubingen, 1930.

[11] E Fermi. Trends to a Theory of beta Radiation. (In Italian). *Nuovo Cim.*, 11:1–19, 1934.

[12] E Fermi. Versuch einer Theorie der β-Strahlen. I. *Zeitschrift für Physik*, 88(3):161–177, 1934.

[13] F. Wilson. Fermi's Theory of Beta Decay. *American Journal of Physics*, 36(12):1150–1160, 1968.

[14] G M Lewis. *Neutrinos*. Wykeham publications, London; Winchester, 1970.

[15] C M G Lattes, et al. Processes Involving Charged Mesons. *Nature*, 159:694–697, 1947.

[16] C M G Lattes, G P S Occhialini, and C F Powell. Observations on the Tracks of Slow Mesons in Photographic Emulsions. 1. *Nature*, 160:453–456,486–492, 1947.

[17] R Brown, et al. Observations With Electron Sensitive Plates Exposed to Cosmic Radiation. *Nature*, 163:82, 1949.

[18] C L Cowan, et al. Large Liquid Scintillation Detectors. *Phys. Rev.*, 90(3):493–494, 1953.

[19] F. Reines and C. L. Cowan. A proposed experiment to detect the free neutrino, 1953.

[20] F. Reines and C. L. Cowan. Detection of the free neutrino. *Physical Review*, 92(3):830–831, 1953.

[21] C L Cowan, et al. Detection of the Free Neutrino: a Confirmation. *Science*, 124(3212):103–104, 1956.

[22] Raymond Davis Jr. and Don S Harmer. Attempt to observe the $Cl^{37}(\bar{\nu}e^{-})Ar^{37}$ reaction induced by reactor antineutrinos. *Bull. Am. Phys. Soc.*, 4:217, 1959.

[23] G Danby, et al. Observation of High-Energy Neutrino Reactions and the Existence of Two Kinds of Neutrinos. *Phys. Rev. Lett.*, 9(1):36–44, 1962.

[24] M. L. Perl, et al. Evidence for anomalous lepton production in e^{+}-e^{-} annihilation. *Physical Review Letters*, 35(22):1489–1492, 1975.

[25] G J Feldman, et al. Inclusive Anomalous Muon Production in $e^{+}e^{-}$ Annihilation. *Phys. Rev. Lett.*, 38(3):117–120, 1977.

[26] J Burmester, et al. Anomalous muon production in $e^{+}e^{-}$ annihilations as evidence for heavy leptons. *Physics Letters B*, 68(3):297–300, 1977.

[27] D. DeCamp, et al. Determination of the number of light neutrino species. *Physics Letters B*, 231(4):519–529, 1989.

[28] B Adeva, et al. A determination of the properties of the neutral intermediate vector boson Z0. *Physics Letters B*, 231(4):509–518, 1989.

[29] M Z Akrawy, et al. Measurement of the Z0 mass and width with the opal detector at LEP. *Physics Letters B*, 231(4):530–538, 1989.

[30] P Aarnio, et al. Measurement of the mass and width of the Z0-particle from multi-hadronic final states produced in $e^{+}e^{-}$ annihilations. *Physics Letters B*, 231(4):539–547, 1989.

[31] S. Schael, et al. Precision electroweak measurements on the Z resonance. *Physics Reports*, 427(5-6):257–454, 2006.

[32] K. Kodama, et al. Observation of tau neutrino interactions. *Physics Letters, Section B: Nuclear, Elementary Particle and High-Energy Physics*, 504(3):218–224, 2001.

[33] H A Bethe. Energy Production in Stars. *Phys. Rev.*, 55(5):434–456, 1939.

[34] John N Bahcall, Neta A Bahcall, and Giora Shaviv. Present Status of the Theoretical Predictions for the ^{37}Cl Solar-Neutrino Experiment. *Phys. Rev. Lett.*, 20(21):1209–1212, 1968.

[35] John N. Bahcall, Aldo M. Serenelli, and Sarbani Basu. New Solar Opacities, Abundances, Helioseismology, and Neutrino Fluxes. *The Astrophysical Journal*, 621(1):L85–L88, 2005.

[36] B. T. Cleveland, et al. Update on the measurement of the solar neutrino flux with the Homestake chlorine detector. *Nuclear Physics B (Proceedings Supplements)*, 38(1-3):47–53, 1995.

[37] John N Bahcall, M H Pinsonneault, and G J Wasserburg. Solar models with helium and heavy-element diffusion. *Rev. Mod. Phys.*, 67(4):781–808, 1995.

[38] J. N. Abdurashitov, et al. Results from SAGE (The Russian-American gallium solar neutrino experiment). *Physics Letters B*, 328(1-2):234–248, 1994.

[39] P. Anselmann, et al. Solar neutrinos observed by GALLEX at Gran Sasso. *Physics Letters B*, 285(4):376–389, 1992.

[40] W. Hampel, et al. GALLEX solar neutrino observations: Results for GALLEX IV. *Physics Letters, Section B: Nuclear, Elementary Particle and High-Energy Physics*, 447:127–133, 1999.

[41] E. Gaisser, T. K.; Engel, R.; Resconi. *Cosmic Rays and Particle Physics*. Cambridge University Press, 1990.

[42] T J Haines, et al. Calculation of Atmospheric Neutrino-Induced Backgrounds in a Nucleon-Decay Search. *Phys. Rev. Lett.*, 57(16):1986–1989, 1986.

[43] K S Hirata, et al. Experimental study of the atmospheric neutrino flux. *Physics Letters B*, 205(2):416–420, 1988.

[44] W Anthony Mann. Atmospheric neutrinos and the oscillations bonanza. *Int. J. Mod. Phys.*, A15S1:229–256, 2000.

[45] B Pontecorvo. Neutrino Experiments and the Problem of Conservation of Leptonic Charge. *Sov. Phys. JETP*, 26:984–988, 1968.

[46] V Gribov and B Pontecorvo. Neutrino astronomy and lepton charge. *Physics Letters B*, 28(7):493–496, 1969.

[47] B Pontecorvo. Mesonium and anti-mesonium. *Sov. Phys. JETP*, 6:429, 1957.

[48] D Casper, et al. Measurement of atmospheric neutrino composition with the IMB-3 detector. *Phys. Rev. Lett.*, 66(20):2561–2564, 1991.

[49] R Becker-Szendy, et al. Electron- and muon-neutrino content of the atmospheric flux. *Phys. Rev. D*, 46(9):3720–3724, 1992.

[50] Y Fukuda, et al. Atmospheric vμve ratio in the multi-GeV energy range. *Physics Letters B*, 335(2):237–245, 1994.

[51] J N Bahcall. Solar Models and Solar Neutrinos. *Physica Scripta*, 2005(T121):46, 2005.

[52] Ziro Maki, Masami Nakagawa, and Shoichi Sakata. Remarks on the Unified Model of Elementary Particles. *Progress of Theoretical Physics*, 28(5):870, 1962.

[53] John N Bahcall, Concepción M Gonzalez-Garcia, and Carlos Pena-Garay. Before and After: How has the SNO NC measurement changed things? *Journal of High Energy Physics*, 2002(07):54, 2002.

[54] A Yu. Smirnov. The MSW effect and solar neutrinos. In *Neutrino telescopes. Proceedings, 10th International Workshop, Venice, Italy, March 11-14, 2003. Vol. 1+2*, pages 23–43, 2003.

[55] L Wolfenstein. Neutrino oscillations in matter. *Phys. Rev. D*, 17(9):2369–2374, 1978.

[56] S P Mikheev and A Yu. Smirnov. Resonance Amplification of Oscillations in Matter and Spectroscopy of Solar Neutrinos. *Sov. J. Nucl. Phys.*, 42:913–917, 1985.

[57] S P Mikheev and A Yu. Smirnov. Resonant amplification of neutrino oscillations in matter and solar neutrino spectroscopy. *Nuovo Cim.*, C9:17–26, 1986.

[58] K Eguchi, et al. First Results from KamLAND: Evidence for Reactor Antineutrino Disappearance. *Phys. Rev. Lett.*, 90(2):21802, 2003.

[59] T Araki, et al. Measurement of Neutrino Oscillation with KamLAND: Evidence of Spectral Distortion. *Phys. Rev. Lett.*, 94(8):81801, 2005.

[60] Abhijit Bandyopadhyay, et al. The Solar neutrino problem after the first results from KamLAND. *Phys. Lett.*, B559:121–130, 2003.

[61] Pedro Cunha de Holanda and A Yu. Smirnov. LMA MSW solution of the solar neutrino problem and first KamLAND results. *JCAP*, 0302:1, 2003.

[62] G L Fogli, et al. Evidence for Mikheyev-Smirnov-Wolfenstein effects in solar neutrino flavor transitions. *Phys. Lett.*, B583:149–156, 2004.

[63] Thomas Mannel. Theory and Phenomenology of CP Violation. *Nuclear Physics B - Proceedings Supplements*, 167:115–119, 2007.

[64] Tommy Ohlsson, He Zhang, and Shun Zhou. Radiative corrections to the leptonic Dirac *CP*-violating phase. *Phys. Rev. D*, 87(1):13012, 2013.

[65] Tommy Ohlsson, He Zhang, and Shun Zhou. Probing the leptonic Dirac CP-violating phase in neutrino oscillation experiments. *Physical Review D - Particles, Fields, Gravitation and Cosmology*, 87(5):1–8, 2013.

[66] DUNE Collaboration. Long-Baseline Neutrino Facility (LBNF) and Deep Underground Neutrino Experiment (DUNE): The LBNF and DUNE Projects. 1, 2016.

[67] K Abe, et al. Physics potential of a long-baseline neutrino oscillation experiment using a J-PARC neutrino beam and Hyper-Kamiokande. *Progress of Theoretical and Experimental Physics*, 2015(5):053C02, 2015.

[68] F Kaether, et al. Reanalysis of the Gallex solar neutrino flux and source experiments. *Physics Letters B*, 685(1):47–54, 2010.

[69] J N Abdurashitov, et al. Measurement of the solar neutrino capture rate with gallium metal. III. Results for the 2002–2007 data-taking period. *Phys. Rev. C*, 80(1):15807, 2009.

[70] B Aharmim, et al. Combined analysis of all three phases of solar neutrino data from the Sudbury Neutrino Observatory. *Phys. Rev. C*, 88(2):25501, 2013.

[71] A Gando, et al. Reactor on-off antineutrino measurement with KamLAND. *Phys. Rev. D*, 88(3):33001, 2013.

[72] R Wendell, et al. Atmospheric neutrino oscillation analysis with subleading effects in Super-Kamiokande I, II, and III. *Phys. Rev. D*, 81(9):92004, 2010.

[73] M G Aartsen, et al. Determining neutrino oscillation parameters from atmospheric muon neutrino disappearance with three years of IceCube DeepCore data. *Phys. Rev. D*, 91(7):72004, 2015.

[74] P Adamson, et al. Measurement of Neutrino and Antineutrino Oscillations Using Beam and Atmospheric Data in MINOS. *Phys. Rev. Lett.*, 110(25):251801, 2013.

[75] P Adamson, et al. Electron Neutrino and Antineutrino Appearance in the Full MINOS Data Sample. *Phys. Rev. Lett.*, 110(17):171801, 2013.

[76] K Abe, et al. Precise Measurement of the Neutrino Mixing Parameter θ_{23} from Muon Neutrino Disappearance in an Off-Axis Beam. *Phys. Rev. Lett.*, 112(18):181801, 2014.

[77] P Adamson, et al. First measurement of muon-neutrino disappearance in NOvA. *Phys. Rev. D*, 93(5):51104, 2016.

[78] M C Gonzalez-Garcia, Michele Maltoni, and Thomas Schwetz. Updated fit to three neutrino mixing: status of leptonic CP violation. *Journal of High Energy Physics*, 2014(11):52, 2014.

[79] Ivan Esteban, et al. Updated fit to three neutrino mixing: exploring the accelerator-reactor complementarity. *Journal of High Energy Physics*, 2017(1):87, 2017.

[80] F P An, et al. Observation of Electron-Antineutrino Disappearance at Daya Bay. *Phys. Rev. Lett.*, 108(17):171803, 2012.

[81] J K Ahn, et al. Observation of Reactor Electron Antineutrinos Disappearance in the RENO Experiment. *Phys. Rev. Lett.*, 108(19):191802, 2012.

[82] K Abe, et al. Observation of Electron Neutrino Appearance in a Muon Neutrino Beam. *Phys. Rev. Lett.*, 112(6):61802, 2014.

[83] P Adamson, et al. First Measurement of Electron Neutrino Appearance in NOvA. *Phys. Rev. Lett.*, 116(15):151806, 2016.

[84] K Abe and Others. First combined analysis of neutrino and antineutrino oscillations at T2K. 2017.

[85] V N Aseev, et al. Upper limit on the electron antineutrino mass from the Troitsk experiment. *Phys. Rev. D*, 84(11):112003, 2011.

[86] Ch Kraus, et al. Final results from phase II of the Mainz neutrino mass search in tritium β-decay. *The European Physical Journal C - Particles and Fields*, 40(4):447–468, 2005.

[87] Planck Collaboration, et al. Planck 2013 results. XVI. Cosmological parameters. *Astronomy & Astrophysics*, 571:A16, 2014.

[88] DUNE Collaboration. Long-Baseline Neutrino Facility (LBNF) and Deep Underground Neutrino Experiment (DUNE): The Physics Program for DUNE at LBNF. 2, 2015.

[89] DUNE Collaboration. Long-Baseline Neutrino Facility (LBNF) and Deep Underground Neutrino Experiment (DUNE): Long Baseline Neutrino Facility for DUNE. 3, 2016.

[90] DUNE Collaboration. Long-Baseline Neutrino Facility (LBNF) and Deep Underground Neutrino Experiment (DUNE): The DUNE Detectors at LBNF. 4, 2016.

[91] S. Amerio, et al. Design, construction and tests of the ICARUS T600 detector. *Nuclear Instruments and Methods in Physics Research, Section A: Accelerators, Spectrometers, Detectors and Associated Equipment*, 527(3):329–410, 2004.

[92] C Anderson, et al. The ArgoNeuT detector in the NuMI low-energy beam line at Fermilab. *Journal of Instrumentation*, 7(10):P10019, 2012.

[93] F Cavanna, et al. LArIAT: Liquid Argon In A Testbeam. 2014.

[94] R Acciarri, et al. Design and construction of the MicroBooNE detector. *Journal of Instrumentation*, 12(02):P02017, 2017.

[95] B Baller, et al. Liquid Argon Time Projection Chamber research and development in the United States. *Journal of Instrumentation*, 9(05):T05005, 2014.

[96] David R Nygren. The Time Projection Chamber - A New 4pi Detector for Charged Particles. *eConf*, C740805(PEP-0144):58–78, 1974.

[97] Carlo Rubbia. The Liquid Argon Time Projection Chamber: A New Concept For Neutrino Detectors.pdf, 1977.

[98] Mitch Soderberg. The MicroBooNE Proposal, 2008.

[99] V Chepel and H Araújo. Liquid noble gas detectors for low energy particle physics. *Journal of Instrumentation*, 8(04):R04001, 2013.

[100] P. Derwent, et al. Proton Improvement Plan-II (PIP-II). Technical Report December, 2013.

[101] Patrick Huber and Joachim Kopp. Two experiments for the price of one? The role of the second oscillation maximum in long baseline neutrino experiments. *Journal of High Energy Physics*, 2011(3):13, 2011.

[102] LBNE Collaboration. Long-Baseline Neutrino Experiment (LBNE) Project: The LBNE Project. 1, 2012.

[103] LBNE Collaboration. Long-Baseline Neutrino Experiment (LBNE) Project: Detectors At The Near Site. 3, 2012.

[104] LBNE Collaboration. Long-Baseline Neutrino Experiment (LBNE) Project: Liquid Argon Detector At The Far Site. 4, 2012.

[105] Margherita Buizza Avanzini. The LAGUNA-LBNO Project. *Physics Procedia*, 61:524–533, 2015.

[106] HEPAP Subcommittee. Building for Discovery: Strategic Plan for U.S. Particle Physics in the Global Context. 2014.

[107] Terry Tope, et al. Extreme argon purity in a large, non-evacuated cryostat. 1169(2014):1169–1175, 2014.

[108] A. Curioni, et al. A regenerable filter for liquid argon purification. *Nuclear Instruments and Methods in Physics Research, Section A: Accelerators, Spectrometers, Detectors and Associated Equipment*, 605(3):306–311, 2009.

[109] Alan Hahn, et al. The LBNE 35 Ton Prototype Cryostat. In *FERMILAB-CONF-14-420-PPD The*, 2014.

[110] David Montanari, et al. First scientific application of the membrane cryostat technology. 1664(2014):1664–1671, 2014.

[111] J. Freeman. Courtesy of John Freeman, Fermilab, 2014.